

# RSC Sustainability

Accepted Manuscript

This article can be cited before page numbers have been issued, to do this please use: S. Dhillon, J. Dziegielowski, P. P. Kundu and M. Di Lorenzo, *RSC Sustain.*, 2023, DOI: 10.1039/D2SU00079B.



This is an Accepted Manuscript, which has been through the Royal Society of Chemistry peer review process and has been accepted for publication.

Accepted Manuscripts are published online shortly after acceptance, before technical editing, formatting and proof reading. Using this free service, authors can make their results available to the community, in citable form, before we publish the edited article. We will replace this Accepted Manuscript with the edited and formatted Advance Article as soon as it is available.

You can find more information about Accepted Manuscripts in the [Information for Authors](#).

Please note that technical editing may introduce minor changes to the text and/or graphics, which may alter content. The journal's standard [Terms & Conditions](#) and the [Ethical guidelines](#) still apply. In no event shall the Royal Society of Chemistry be held responsible for any errors or omissions in this Accepted Manuscript or any consequences arising from the use of any information it contains.

Sustainability Spotlight Statement

View Article Online  
DOI: 10.1039/D2SU00079B

We are facing unprecedented times of crisis on multiple fronts. Energy demands are rising to respond to the needs of an ever-expanding population that poses seriously threats to the resilience of cities. Land pollution is one of the sad outcomes of this situation. Soil microbial fuel cell technology provides a very attractive opportunity for clean and emission-free energy production and sustainable bioremediation of contaminated soil. In this study, we investigate on the use of carbon-based composite electrode materials to enhance the electrochemical performance of this technology and help its progress towards practical implementations. Our work is primarily aligned with the UN SDGs 7, 11, but it is also related to the UN SDGs 15 and 13.



## Functionalised graphite felt anodes for enhanced power generation in membrane-less soil microbial fuel cells

Simran Kaur Dhillon<sup>1,2</sup>, Jakub Dziegielowski<sup>1</sup>, Patit Paban Kundu<sup>2\*</sup>, Mirella Di Lorenzo<sup>1\*</sup>

<sup>1</sup> Department of Chemical Engineering and Centre for Biosensors, Bioelectronics & Biodevices (C3Bio), University of Bath Claverton Down, BA2 7AY, UK

<sup>2</sup> Department of Chemical Engineering, Indian Institute of Technology, Roorkee, 247667, India

Corresponding authors: [m.di.lorenzo@bath.ac.uk](mailto:m.di.lorenzo@bath.ac.uk), [patit.kundu@ch.iitr.ac.in](mailto:patit.kundu@ch.iitr.ac.in)

### Abstract

There is a global need for sustainable and clean technologies that can actively contribute to reach the net-zero carbon goal by 2050. Soil microbial fuel cell (SMFC) technology has a huge potential as affordable and green energy harvesting source and as a carbon-neutral bioremediation strategy for the treatment of pollutant lands. In this work, for the first time the use of cobalt oxide modified graphite felt (GF) electrodes is explored as the anode material in SMFCs, with the aim of promoting the development of a high-performing electroactive biofilm and, therefore, boosting the electrocatalytic processes. Cobalt oxide (Co<sub>3</sub>O<sub>4</sub>) nanoflowers, obtained by calcinating cobalt hydroxide salt hydrothermally deposited onto graphite felt, decreased the hydrophobicity, the conductivity and consequently the electrochemical activity of carbon-based electrodes. Physiochemical characterisation studies revealed that the cobalt nanostructures were uniformly deposited and anchored onto the GF electrode. Nonetheless, when Co<sub>3</sub>O<sub>4</sub>-GF anodes were tested in a membrane-less, air-cathode SMFC device, after an initial boost in power performance, the activity decayed with time, probably due to Co<sub>3</sub>O<sub>4</sub> leaching. Interweaving of Co<sub>3</sub>O<sub>4</sub> functionalised GF electrodes with polyaniline (PANI) (PANI-Co<sub>3</sub>O<sub>4</sub>-GF anode), led to a highly performing SMFC system that generated a peak power density of 70 mW m<sup>-2</sup>, corresponding to a current density of 143 mA m<sup>-2</sup>. This value of power density was nearly three times greater than the power generated by the same SMFC system but with a plain GF anode. The interweaving of PANI onto the Co<sub>3</sub>O<sub>4</sub>-GF electrode led to a porous structure that, while favouring microbial attachment, provides stability to the electrode over prolonged periods of operation. Overall, these results



provide exciting perspectives on the development of composite carbon-based anode materials for highly performing soil microbial fuel cells, thus inspiring future trends in the field.

## 1. INTRODUCTION

To contrast the devastating effects of climate change, we must increase our reliance on low-carbon emission technologies and move away from fossil fuels. According to the World Economic Forum, decarbonization, the reduction of carbon dioxide emissions resulting from human activity in the atmosphere, is the only solution to climate stabilization. Microbial fuel cell technology can help address this global emergency by providing a net-zero carbon, sustainable and cost-effective solution <sup>1</sup>. Microbial fuel cell technology generates electricity through microbial degradation of organic substrates from low-value energy sources, including wastewaters, to H<sub>2</sub>O and CO<sub>2</sub> <sup>2</sup>. Amongst the several types of microbial fuel cell designs, soil microbial fuel cells (SMFCs) are particularly attractive, given the simplicity of design, the long-term stability and the minimum maintenance required, which facilitates remote applications <sup>3</sup>. SMFCs also offer attractive perspectives on self-powered soil bioremediation <sup>4</sup>; organic pollutants in soils are degraded at the anode via the action of endogenous microorganisms, and the electrons generated throughout the process are transported to the cathode via an external circuit, thus producing electricity. At the cathode, the electrons participate in the oxygen reduction reaction (ORR) together with the protons generated at the anode and transferred to the cathode across the soil matrix <sup>5</sup>. As the redox reactions proceed at the electrodes, a potential gradient develops, favouring power generation and bioremediation processes <sup>6</sup>. Soil characteristics, such as availability of liable organics, endogenous microbial communities, water content, and pH, markedly influence the electrochemical performance of the SMFC <sup>5</sup>. Design factors, such as electrode configuration and orientation, also influence the electroactive efficiency of SMFCs <sup>7</sup>.

The anode material influences the development of the electroactive biofilm and, therefore, the overall performance of the SMFC <sup>8</sup>. Carbonaceous materials, including carbon paper, carbon felt, and graphite felt, have been extensively exploited in microbial fuel cells <sup>9–11</sup>. Carbon electrodes are preferred over metal-based ones in microbial fuel cells due to their high biocompatibility, specific surface area and roughness that promote attachment and growth of biofilm, as well as guaranteeing the cost-effectiveness of the resulting device <sup>12–14</sup>. In SMFCs,



carbon-based additives such as biochar<sup>15</sup> and carbon fibers<sup>16</sup> are added to the soil to overcome charge transfer limitations. Graphite felt (GF) is a particularly popular electrode material in microbial fuel cells due to its 3D structure with high specific surface area<sup>17</sup>. A recent study compared the performance of SMFC with graphite felt as cathode against different anodes such as graphite felt, aluminium sheet, activated carbon felt, graphite paper, and carbon cloth. After 115 days of continuous operation, SMFC with graphite felt as the cathode and anode electrode, generated the greatest cell potential and power density compared to other 2D electrodes<sup>18</sup>. Nonetheless, GF has greater hydrophobicity compared to other carbon-based electrodes, which can limit microbial attachment and the effective development of electroactive biofilm<sup>19</sup>. Consequently, GF electrodes are typically acid treated to allow protonation of -OH group onto the electrode surface and enhance electrostatic interactions<sup>20</sup>. The conductivity of carbon-based anodes can be enhanced with the use of metals<sup>21</sup>. For example, the functionalization of graphite felt with Fe<sub>3</sub>O<sub>4</sub> and bentonite-Fe, led to a power density generated by the SMFC respectively 2 times and three times higher than the case of pure graphite felt anodes<sup>22</sup>. Composite materials, consisting of carbon and transition metals such as Fe, Co, Ni, Fe, and Cu, offer an attractive anode material alternative for microbial fuel cells since they combine the benefits of carbon-based materials with the great conductivity of metal oxides for high electron transfer rates<sup>23–25</sup>. Among the several options, cobalt oxide is particularly promising as an anode material, as it has been shown to reduce the hydrophobicity of GF and improve the interfacial charge transfer rates<sup>26–27</sup>. These benefits result from an enhanced specific surface area of the electrode thanks to the 3D structure of the Co<sub>3</sub>O<sub>4</sub> nanoflowers combined with the generation of positively charged metal catalytic sites that promote the adhesion of negatively charged bacteria onto the electrode surface<sup>28</sup>.

In the development of carbon-metal composite electrode materials, porous conducting polymers can provide a matrix for the entrapment of the metal catalyst and/or support that prevents leaching and enhance stability while enhancing electronic and ionic conductivity<sup>29</sup>. In particular, polyaniline (PANI) modified composites have been widely used in microbial fuel cells<sup>30–32</sup>. The interweaving of PANI with metals or metal oxides leads to conducting nanocomposites that, compared to conventional carbon electrodes, have a larger surface area, better catalytic activity, and, thus, can lead to better performing microbial fuel cells<sup>33</sup>.



In this study, we explore the use of graphite felt functionalized with cobalt oxide nanoflowers as the anode material in SMFCs. The cobalt oxide nanoflowers are obtained by calcinating cobalt hydroxide salt hydrothermally deposited onto graphite felt. The performance of the resulting  $\text{Co}_3\text{O}_4$ -GF electrode as the anode of an air-cathode and membrane-less SMFC is investigated and compared with a second type of composite anode material in which the  $\text{Co}_3\text{O}_4$  nanoflowers on GF are embedded within a polyaniline structure (PANI- $\text{Co}_3\text{O}_4$ -GF). To overcome the risk of poor electron transfer efficiency<sup>34</sup>, PANI can enhance the roughness of the electrode<sup>35</sup>, which has been reported as crucial for anode performance in microbial fuel cells<sup>36,37</sup>. Moreover, the positively charged PANI would attract negatively charged microorganisms at the anode facilitating their attachment<sup>38</sup>; PANI has been shown to allow direct electron transfer to the anode via redox centers in the outer membrane and mediators excreted by electroactive species like *Shewanella oneidensis*<sup>39,40</sup>. To the best of our knowledge, this is the first example of using a composite anode material, consisting of a conductive polymer and a transition metal oxide, in a soil microbial fuel cell system. The two composite anode electrodes, along with two controls, GF coated with PANI (PANI-GF) and GF, are physically and electrochemically characterized. This work paves the way for future directions on composite anode materials based on cost-effective metal derivatives for highly performing SMFC systems.

## 2. MATERIALS AND METHODS

### 2.1 Materials

All the reagents used were purchased from Sigma Aldrich of analytical grade and used without further purification.  $\text{Co}(\text{NO}_3)_2 \cdot 6\text{H}_2\text{O}$  was purchased from Sigma-Aldrich. Aniline  $\geq 99.5\%$  and ammonium peroxodisulphate (APS)  $\geq 98\%$  were purchased from VWR chemicals. Graphite felt was purchased from Online Furnace Services Ltd. Scotland, UK. All aqueous solutions were prepared in deionised water.

The soil used in the study was collected from the University of Bath campus. No additives were used to improve the soil quality. After collection, the soil was manually sieved and cleaned of small stones, roots, and leaves. **Table 1** summarises the properties of the soil used. HI-3869 Soil test kit by Hanna Instruments was to test the elemental content, particularly nitrogen (N), phosphorous (P), and potassium, for soil quality analysis (soil test interpretation guide). The conductivity and pH of the soil were determined using a Thermo Scientific Orion Star A325 probe



before the operation. To determine the moisture content of the soil, a measured amount of soil was oven dried at 105°C for 24 h and the difference in the initial weight of the soil and the weight after thermal treatment was used according to Equation 1.

$$\% \text{ Moisture content} = \left( \frac{\text{initial weight} - \text{final weight}}{\text{final weight}} \right) \times 100 \quad \text{Equation 1}$$

After moisture content analysis, the dried sample was further heated in a muffle furnace at 350°C for another 24 h to obtain the organic matter content according to Equation 2<sup>3</sup>.

$$\% \text{ Organic content} = \left( \frac{W_{105} - W_{350}}{W_{105}} \right) \times 100 \quad \text{Equation 2}$$

Where  $W_{105}$  (g) is the weight of soil obtained after drying at 105°C and  $W_{350}$  is the final weight (g) after drying at 350°C.

**Table 1.** Physicochemical parameters of soil used for laboratory studies.

Parameters	Measured values from laboratory tests
pH	6.8
Conductivity	1084 $\mu\text{S cm}^{-1}$
Nitrogen content	High
Phosphorous content	Low
Potassium content	Medium
Moisture content	28.75%
Organic matter content	5.52

## 2.2. Preparation of functionalized graphite felt anodes

Before modification, graphite felt (7 cm × 7 cm) was thoroughly washed by sequentially soaking into 1 M HCl, 3% H<sub>2</sub>O<sub>2</sub> and distilled water at 60°C for 30 min each, and finally heated at 450°C. Flower-like Co<sub>3</sub>O<sub>4</sub> nanostructures were synthesized onto GF via a two-stage hydrothermal-calcination process, following previous work<sup>41</sup>. The resulting GF pieces were soaked in an aqueous solution containing 0.44 g of Co(NO<sub>3</sub>)<sub>6</sub>H<sub>2</sub>O and 0.42 g of urea and sonicated for 30 minutes to ensure a uniform concoction. The electrode suspension was transferred to a Teflon-





lined hydrothermal reactor (150 mL) and maintained at 120°C for 6 h in a hot-air oven. After cooling to room temperature, the GF pieces coated with cobalt hydroxide were carefully rinsed in distilled water and dried at 60°C. Finally, calcination was performed at 300°C in a muffle furnace for 3 h to obtain GF coated with  $\text{Co}_3\text{O}_4$  nanoflowers ( $\text{Co}_3\text{O}_4$ -GF) (**Figure 1a**). **Figure 1b** and **1c** provide respectively an overview of the electrodes tested in this study and the experimental set-up,.

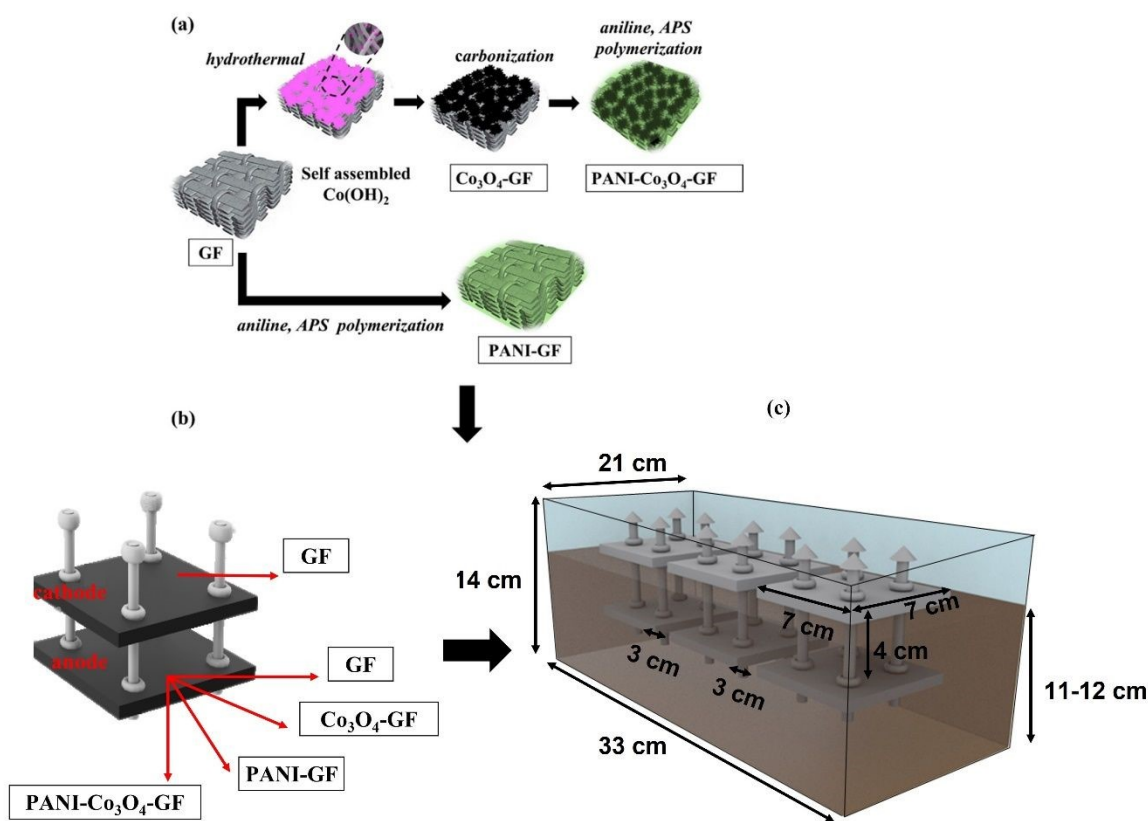


**Figure 1.** Synthesis steps for the electrodes developed (a); SMFC design and overview of the electrodes tested in this study (b); and experimental set-up (c).

PANI- $\text{Co}_3\text{O}_4$ -GF electrode was prepared by electro-polymerization of aniline onto the surface of  $\text{Co}_3\text{O}_4$ -GF electrodes in a three-electrode cell with stainless steel mesh (7 cm  $\times$  7 cm) as the counter for an unhindered flow of electrons and Ag/AgCl as the reference electrode, respectively, using PalmSens4 potentiostat equipped with the PSTrace software. First, the surface





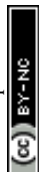
of the  $\text{Co}_3\text{O}_4$ -GF electrode was activated by cyclic voltammetry (CV) at  $50 \text{ mV s}^{-1}$  for 5 cycles in a  $0.7 \text{ M HNO}_3$  aqueous solution. Then,  $0.4 \text{ M}$  aniline was added to the acidic solution, followed by  $\text{N}_2$  purging for 30 minutes before electro-polymerization. The synthesis was initiated by chronoamperometry at  $0.75 \text{ V}$  for 30 minutes<sup>42</sup>. The resulting electrode was rinsed with dilute HCl and distilled water to remove any impurities and dried overnight.

PANI-GF electrodes were also tested as a control. In this case, PANI was electro-polymerized (following the method described above) onto GF electrode not functionalized with  $\text{Co}_3\text{O}_4$ .

## 2.3 Material characterization and electrochemical analysis

The structure of the generated electrodes was analyzed by X-ray diffraction (XRD, STOE STADI P), while Fourier Transform-Infrared spectroscopy (Perkin Elmer FT-IR spectrometer) was performed to identify the surface functionalities of the electrodes within the wavelength range of  $400\text{--}4000 \text{ cm}^{-1}$ . Scanning electron microscopy (SEM, Hitachi SU3900) and elemental mapping were used to assess electrode material morphology and elemental distribution. The electrodes were gold-coated before the analysis. ImageJ software was used to analyse the SEM images generated. Contact angle measurements (DataPhysics OCA 25) were taken to assess the hydrophobicity of the electrodes. To examine the morphology of the anodic biofilm, the several anodes after 4 months of operation were conditioned with 4% glutaraldehyde solution for 4 h, followed by dehydration in different concentrations of ethanol solution (25%, 50%, 75%, and 100%) at room temperature, each for 15 min<sup>43</sup>. The air-dried anodes were coated with gold by sputtering and analysed by SEM.

The electrochemical performance of the electrodes developed as the anode in an SMFC was investigated at different stages of batch operation by using Ag/AgCl as the reference electrode and the SMFC cathode (plain GF) as the counter electrode. Before testing, the working electrode was cycled at  $0.01 \text{ V s}^{-1}$  within the potential window  $-0.5 \text{ V}$  to  $1 \text{ V}$  for at least 15 min before data collection. Cyclic voltammetry (CV) and linear sweep voltammetry (LSV) measurements were recorded. Further, the stability of the electrodes developed was determined by chronoamperometry (CA) at  $0.25 \text{ V}$  for 30 minutes after 30 days of operation to examine the effect of biofilm adhesion onto the electrode surface. Electrochemical impedance spectroscopy (EIS) was carried in the frequency range  $105 \text{ Hz}$  to  $0.1 \text{ Hz}$  to assess the ohmic and charge transfer



resistances of the several electrodes produced prior to be used as the anode in the SMFC. Tests were performed in a three-electrode set-up in 50 mM PBS, using the anode as the working electrode, Pt wire as the counter electrode and Ag/AgCl electrode as the reference electrode. EIS measurements were also repeated after four months of operation to assess the effect that the anodic biofilm has on the electrode resistance. In this case, the tests were done directly in the soil media where the SMFCs were operated, with the anode as the working electrode, the GF cathode as the counter electrode, and Ag/AgCl electrode as the reference electrode.

## 2.4 Soil microbial fuel cell configuration and operation

Air-cathode, membrane-less SMFCs, which differed according to the anode material used, were constructed as previously described<sup>3</sup>. Briefly, the system consisted of an anode (7 x 7 cm), either GF, Co<sub>3</sub>O<sub>4</sub>-GF, PANI-Co<sub>3</sub>O<sub>4</sub>-GF, or PANI-GF, buried inside the soil, and a cathode (7 x 7 cm), made of untreated GF, placed onto the soil surface at a fixed distance from the anode of 4 cm, and exposed to air. Rectangular PVA containers (33 cm × 21 cm × 14 cm), filled with approximately 7-8 Kg soil, were used to host three replicates of a specific SMFC type for a total of four PVA containers and 12 SMFCs tested. The moisture content in soil is a key factor for SMFC operation<sup>3,44</sup>. Accordingly, approximately 250 mL of tap water was sprinkled over the topsoil layer on a two-day basis to compensate for moisture loss due to evaporation. This helps maintain water saturation condition in the soil while ensuring that the cathodes are not submerged in water. Titanium wire (0.25 mm, Alfa Aesar) intertwined within the electrodes was used to connect the anode and cathode to an external resistance of 510 Ω. Voltage drops (V) across each SMFC were recorded and collected using a data acquisition system (DAQ6510, Keithley instruments, Tektronix UK Ltd.). Polarization tests were conducted by first operating the SMFCs under open circuit voltage for 12 h and then applying decreasing external loads (R), from 10000 Ω, 5000 Ω, 1000 Ω, 700 Ω, 500 Ω, 300 Ω, and 100 Ω, at 10 min intervals using a resistor box (Cropico resistance decade box, resistance range 10M Ω-10 Ω) and recording the output voltage and current. Current density (mA cm<sup>-2</sup>) was calculated according to Ohm's law;  $I = V/(RA)$ , where V is the cell voltage (V) and A is the geometric anode area (49 cm<sup>2</sup>). Power density (mW cm<sup>-2</sup>) was calculated as  $P = (IV)/A$ .

## 3. RESULTS AND DISCUSSION

### 3.1. Physicochemical characterizations of the anodes developed



In this study, four different types of graphite felt electrodes were tested as the anode in an air-cathode and membrane-less soil microbial fuel cell: plain graphite felt (GF), graphite felt coated with polyaniline (PANI-GF), graphite felt functionalized with cobalt oxide nanoflowers ( $\text{Co}_3\text{O}_4$ -GF), graphite felt functionalized with cobalt oxide nanoflowers and coated with polyaniline (PANI- $\text{Co}_3\text{O}_4$ -GF). The hydrophobicity of the four electrodes was investigated and compared. As expected, the functionalization of graphite felt with  $\text{Co}_3\text{O}_4$  led to a decrease in the hydrophobicity, corresponding to a reduction of the contact angle to  $116 \pm 0.6^\circ$  from a value of  $139 \pm 0.1^\circ$  for plain GF (**Figure 2a**). This improvement in the electrode wettability could result from the oxygen atoms introduced by  $\text{Co}_3\text{O}_4$  that could alter the electrostatic field at the surface of graphite felt and facilitate interaction between the electrode material and water molecules<sup>45,28</sup>. The electrodeposition of PANI further decreased the surface hydrophobicity, with PANI- $\text{Co}_3\text{O}_4$ -GF reaching a contact angle of  $97 \pm 0.9$ . The decrease in the electrode hydrophobicity resulting from the synergistic effect of  $\text{Co}_3\text{O}_4$  and PANI, along with the porosity and high specific surface area achieved, promotes good contact between electroactive biofilm and anode, thus enhancing electron transfer<sup>46,47</sup>.

FTIR spectroscopy analysis of the four electrodes was also carried out. **Figure 2b** shows the spectra obtained for each anode material. All electrodes exhibit similar peaks over the wavenumber range  $500 - 4000 \text{ cm}^{-1}$ , which are associated with GF. However, the intensity of the peaks varied significantly with the surface modifications introduced. For all electrodes, absorption bands observed at around  $1020 \text{ cm}^{-1}$  (-CO),  $1110 \text{ cm}^{-1}$  (-COOH),  $1640 \text{ cm}^{-1}$  (-C=O),  $2855 \text{ cm}^{-1}$  (-CH),  $2918 \text{ cm}^{-1}$  (-CH), and  $3377 \text{ cm}^{-1}$  (-OH), belong to stretching vibrations of hydroxyl and carboxyl groups<sup>48</sup>. The peaks observed at  $1579 \text{ cm}^{-1}$  and  $1476 \text{ cm}^{-1}$  in the case of PANI-GF and PANI- $\text{Co}_3\text{O}_4$ -GF are associated with C=C stretching vibrations of benzene and quinone rings due to polyaniline oxidation. Distinct peaks in the range  $650 - 500 \text{ cm}^{-1}$  indicate tetrahedral and octahedral occupancies of metal (M)-O bonds formed with the deposition of  $\text{Co}_3\text{O}_4$  on GF electrodes, which suggests the formation of Co-O moieties in  $\text{Co}_3\text{O}_4$ -GF and PANI- $\text{Co}_3\text{O}_4$ -GF<sup>49</sup>. The absorption band of C-H bending peaks for PANI shifts to higher peak positions in PANI- $\text{Co}_3\text{O}_4$ -GF, which suggests a strong interaction between interweaved PANI and  $\text{Co}_3\text{O}_4$  nanostructures on GF<sup>42</sup>. Further, the broadening of the peak at  $1306 \text{ cm}^{-1}$  confirms the formation of a coordination compound between cobalt ions and amine/imine-nitrogen groups of PANI and enhanced charge delocalization on PANI with the incorporation of transition metal ions<sup>50</sup>.



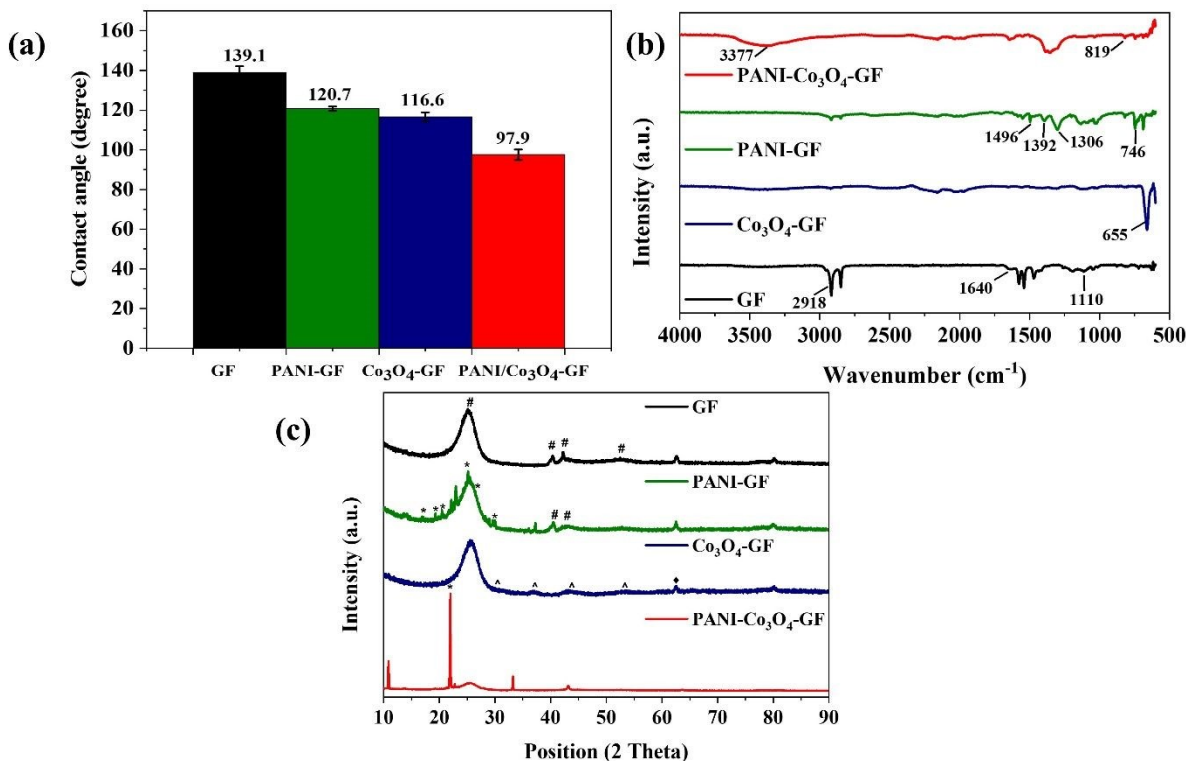


**Figure 2.** Physiochemical analyses of the four anodes tested in this study. (a) Contact angle measurements. Error bars account for the deviation in the measured angle at three different points on the electrode surface. (b) FTIR spectra. (c) XRD analysis

**Figure 2c** shows the XRD patterns for the four electrodes investigated. As shown, distinct diffraction patterns are observed at around 25.05°, 42.82°, 43.24°, and 52.48° assigned respectively to (002), (100), (101), and (102) planes of graphite (#)<sup>51</sup>. Other carbon planes are observed at 37.24°, 62.64°, and 80.20°, which correspond to the turbostratic structure of carbon (JCPDS No. 10-074-2330). The broad reflection from the (002) plane indicated the deprived crystallinity of GF<sup>52</sup>. The XRD spectrum for PANI-GF shows good crystallinity. In addition to the peaks of GF, new diffractions are observed at around 16.90° (011), 19.33°/20.49° (020), 25.16° (200), 27.39° (121), and 30.01° (022), which are assigned to reflection from (011), (020), (200), (121), and (022) planes of PANI (\*)<sup>53,54</sup>. Among these, the observed peaks at 19.33° and 25.16° correspond to the periodicity parallel and perpendicular to the long polymeric chains of PANI, suggesting a partially crystalline nature of the polymer<sup>55</sup>. The XRD spectrum for Co<sub>3</sub>O<sub>4</sub>-GF indicates reflections at 31.41°, 36.6°, 44.3°, and 54.54° attributed respectively to (220), (311), (400), and (422) planes of cobalt (II,III) oxide; Co<sub>3</sub>O<sub>4</sub> (^) (JCPDS No. 00-074-1657)<sup>56</sup>. The weak



reflection at  $62.54^\circ$  is attributed to the (220) plane of cobalt (II) oxide; CoO ( $\blacklozenge$ ) (JCPDS card no. 43-1004) <sup>57</sup>. The presence of Co<sub>3</sub>O<sub>4</sub> peaks in the XRD spectrum for PANI-Co<sub>3</sub>O<sub>4</sub>-GF suggests that electro polymerization of PANI does not alter the crystalline structure of Co<sub>3</sub>O<sub>4</sub>. GF modified with cobalt oxide could act as an efficient platform to improve the anode mass transfer efficiency by enhancing the extracellular electron transfer in SMFCs, considering the excellent capacitive property of Co<sub>3</sub>O<sub>4</sub>-GF that would act as an internal capacitor by accumulating the charge produced by the biofilm during the cell operation <sup>58</sup>. Sharp peaks at around  $20^\circ$  and  $22.46^\circ$  correspond to (110) and (003) lattice planes of PANI, respectively, confirming the amorphous state of the polyaniline deposited <sup>59</sup>.





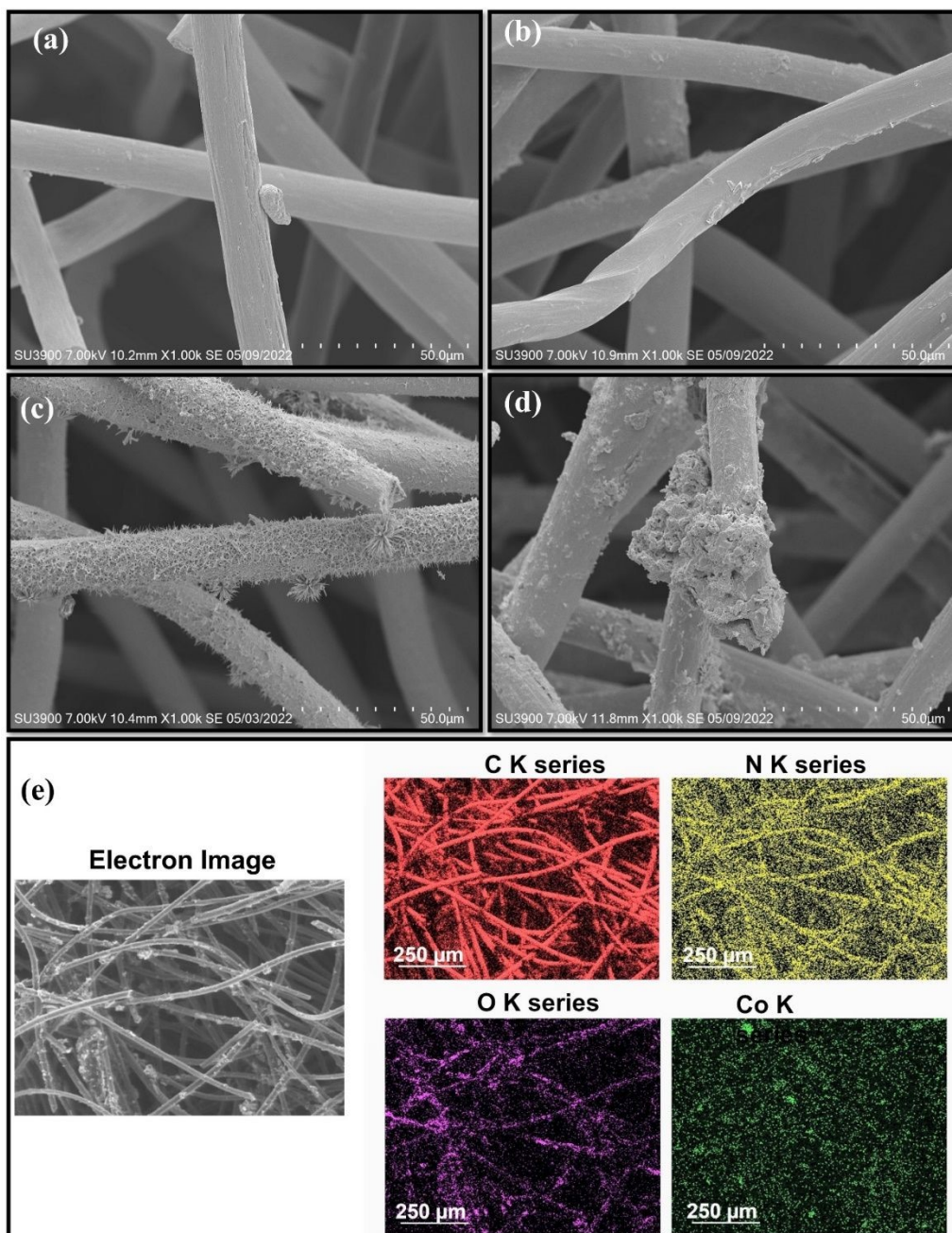


**Figure 3.** SEM images of GF (a), PANI-GF (b), Co<sub>3</sub>O<sub>4</sub>-GF (c) PANI-Co<sub>3</sub>O<sub>4</sub>-GF (d) electrodes and elemental mapping of PANI-Co<sub>3</sub>O<sub>4</sub>-GF (e).

SEM images of the four electrodes show structure changes. Despite harsh etching with acid and H<sub>2</sub>O<sub>2</sub>, GF fibers exhibit a smooth surface, which could be attributed to limited oxidation ability of peroxide (**Figure 3a**). The average diameter of the microfibers increases from 13.1 μm for GF



to 35.4  $\mu\text{m}$  for PANI-GF, confirming the polymer deposition onto the GF fibers (**Figure 3b**).  $\text{Co}_3\text{O}_4$ -GF shows a characteristic 3D flower-like nanostructure anchored on the GF fibers, which consists of many nanowires mounted together with sharp edge (**Figure 3c**). Although the incorporation of transition metal oxides can enhance the electrical conductivity of anode electrodes, they are typically characterised by a smooth surface and by poor corrosion resistance, which prevent the development of a good microbial biofilm<sup>60,61</sup>. The interweaving of PANI and  $\text{Co}_3\text{O}_4$ -GF reveals a significant change in the electrode morphology, with a large density of defect sites, high porosity, and a rough surface that markedly enhance the electrode surface area (**Figure 3d**). Microbial adhesion and charge diffusion are expected to be enhanced in PANI- $\text{Co}_3\text{O}_4$ -GF<sup>62</sup>. The elemental mapping of PANI- $\text{Co}_3\text{O}_4$ -GF is assessed by energy dispersive X-ray spectroscopy (EDS) (**Figure 3e**). As seen, cobalt, oxygen and nitrogen are uniformly distributed on the carbon matrix, thus suggesting that  $\text{Co}_3\text{O}_4$  nanoflowers onto the GF surface are covered by PANI with no phase segregation<sup>63</sup>. Interweaving of PANI provides stability to  $\text{Co}_3\text{O}_4$  by enhancing the interlayer distance to accommodate high ion density, thus increasing the specific capacity of the resulting composite electrode<sup>64</sup>. The elemental composition of PANI- $\text{Co}_3\text{O}_4$ -GF is detailed in **Table S1**.

### 3.2. Electrochemical performance of the anode electrodes developed

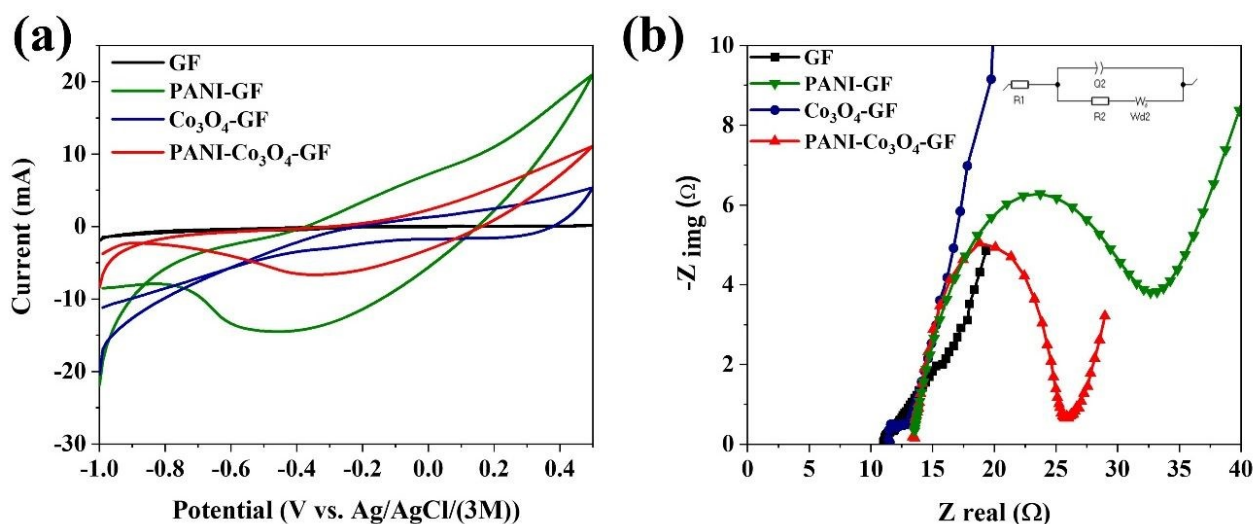


**Figure 4.** Electrochemical characterisation of the anode electrodes before use. (a) CV scans at 0.01  $\text{V s}^{-1}$  and (b) EIS spectra. Tests were performed in a 3-electrode system in 50 mM PBS (pH 7), with the anode as the working electrode and Pt wire (diameter: 0.127 mm) as the counter electrode.





CV scans of the modified anodes prior to use in the SMFCs (**Figure 4a**), revealed that PANI-GF generates the higher current density and CV curve area. This result suggests that the deposition of porous polyaniline enhances the double layer capacitance of the carbon electrode, with an increase in the charge storage <sup>65</sup>. PANI-Co<sub>3</sub>O<sub>4</sub>-GF shows a high redox potential, which could be a consequence of the synergistic effect of Co<sub>3</sub>O<sub>4</sub> and PANI; this modification enhances the surface area of the electrode and its catalytic activity due to an increase in the density of active sites available for the redox reactions at anode and an enhancement in the ion/electron diffusion rate <sup>66, 67,68</sup>.

EIS spectra for the modified anodes were fitted to an equivalent circuit (**Figure 4b**), consisting of ohmic resistance ( $R_1$ ), charge transfer (or polarisation) resistance ( $R_2$ ), constant phase element (Q), and Warburg resistance (W) <sup>69</sup>. The ohmic resistance was recorded around 11.05-13.55  $\Omega$ . The charge transfer resistance was highest for PANI-GF, followed by PANI- Co<sub>3</sub>O<sub>4</sub>-GF, GF and Co<sub>3</sub>O<sub>4</sub>-GF. The high charge transfer resistance of PANI-GF could be a consequence of the steric hindrance towards ions induced with the deposition of polyaniline on graphite felt. PANI may hinder electron hopping, thus increasing the transition energy and decreasing the conductivity of the composite electrode, leading to high resistance <sup>70, 71</sup>. Co<sub>3</sub>O<sub>4</sub>-GF showed the lowest resistance to charge transfer and good pseudo-capacitance for charge storage, which could be attribute to the extended surface area and high conductivity of Co<sub>3</sub>O<sub>4</sub> that facilitate ion transport in the electrolyte <sup>72</sup>.



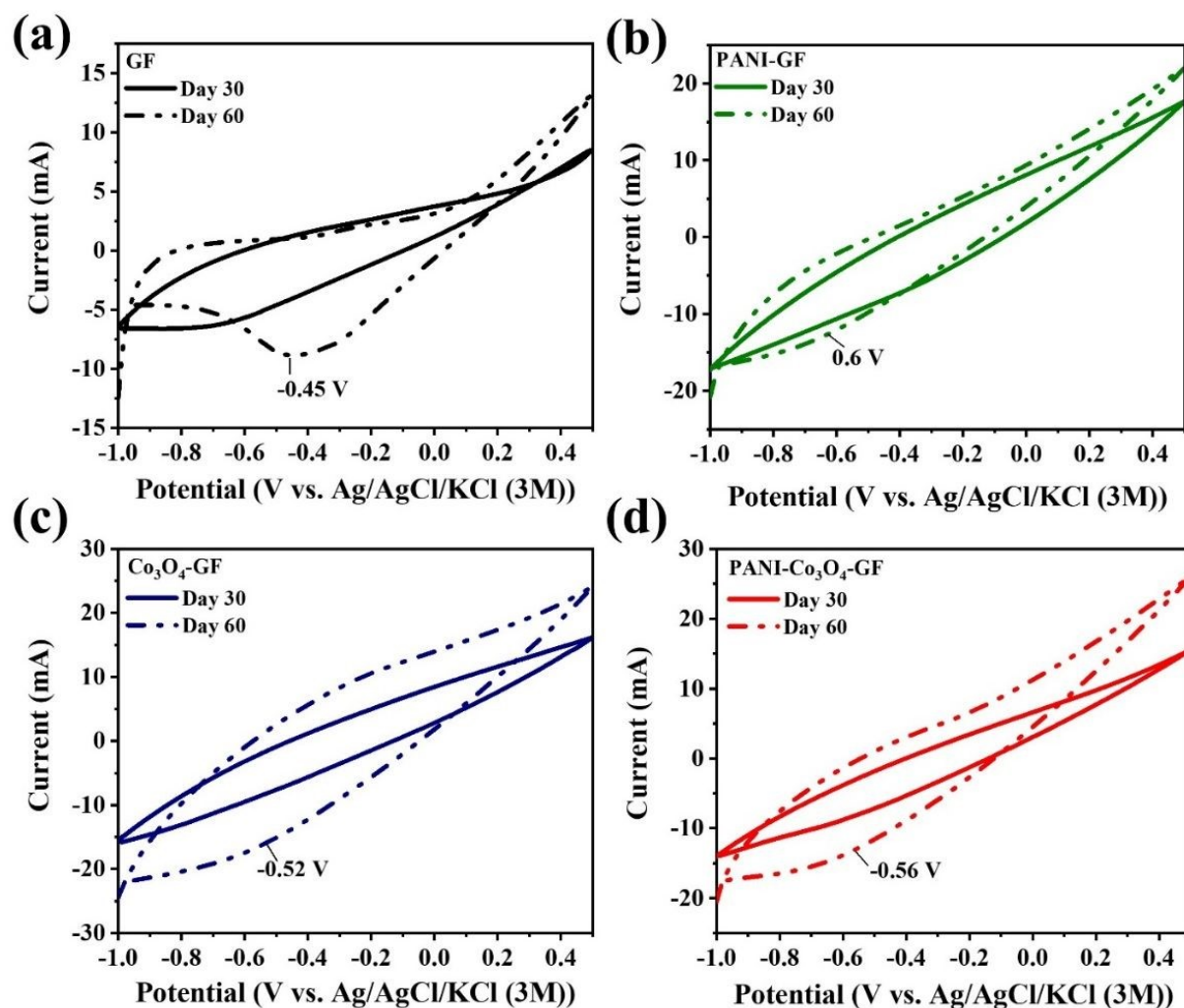


**Figure 5.** Comparison of CV scans at  $0.01 \text{ V s}^{-1}$  obtained with the anode tested in SMFCs operated under 30 and 60 days. (a) GF; (b) PANI-GF; (c)  $\text{Co}_3\text{O}_4$ -GF; (d) PANI- $\text{Co}_3\text{O}_4$ -GF. Values are averages calculated from 3 replicate anodes with a maximum standard deviation of  $\pm 6.1 \text{ mA}$ ,  $\pm 2.4 \text{ mA}$ ,  $4.5 \text{ mA}$  and  $4 \text{ mA}$ , respectively.

The catalytic activity of the biofilms on the anode electrodes was examined in SMFCs, implementing the four types of anodes in triplicate. The redox behaviour of the biofilm developed onto the anode surface after 7, 30 and 60 days of operation was electrochemically characterized by CV. As shown in **Figure S1**, the CV curve recorded after 7 days of operation did not show any electrochemical activity. However, the high current magnitudes and the increased CV curve area compared to GF suggest a superior electrochemical activity of modified anodes<sup>73</sup>. The electrocatalytic activity of the biofilms formed onto several anode materials was tested after 30



and 60 days of SMFC operation. An increase in the CV curve area was observed for all electrodes, along with a rise in the capacitive current of the electrodes over time (**Figure 5**). The CV surface area improvement indicates better extracellular electron transfer between the anode and the microbial biofilm<sup>62</sup>. PANI-GF exhibits an oxidation peak at -0.6 V, PANI-Co<sub>3</sub>O<sub>4</sub>-GF at 0.56 V, Co<sub>3</sub>O<sub>4</sub>-GF at 0.52 V, and GF at 0.45 V, respectively. The peak current of PANI-Co<sub>3</sub>O<sub>4</sub>-GF was 12.12 mA, while Co<sub>3</sub>O<sub>4</sub>-GF recorded a current of 16.03 mA, followed by PANI-GF at 12.37 mA and GF at 8.83 mA. Compared to Co<sub>3</sub>O<sub>4</sub>-GF, the catalytic activity of PANI-Co<sub>3</sub>O<sub>4</sub>-GF was slightly lower. The highest peak and limiting current for Co<sub>3</sub>O<sub>4</sub>-GF suggests that Co<sub>3</sub>O<sub>4</sub>-GF could be a potential charge reservoir for efficient electron transfer due to its electrocapacitive behaviour<sup>74</sup>. Compared to Co<sub>3</sub>O<sub>4</sub>-GF, PANI-Co<sub>3</sub>O<sub>4</sub>-GF exhibits a lower capacitance and a greater electrochemical surface area (in terms of CV area).

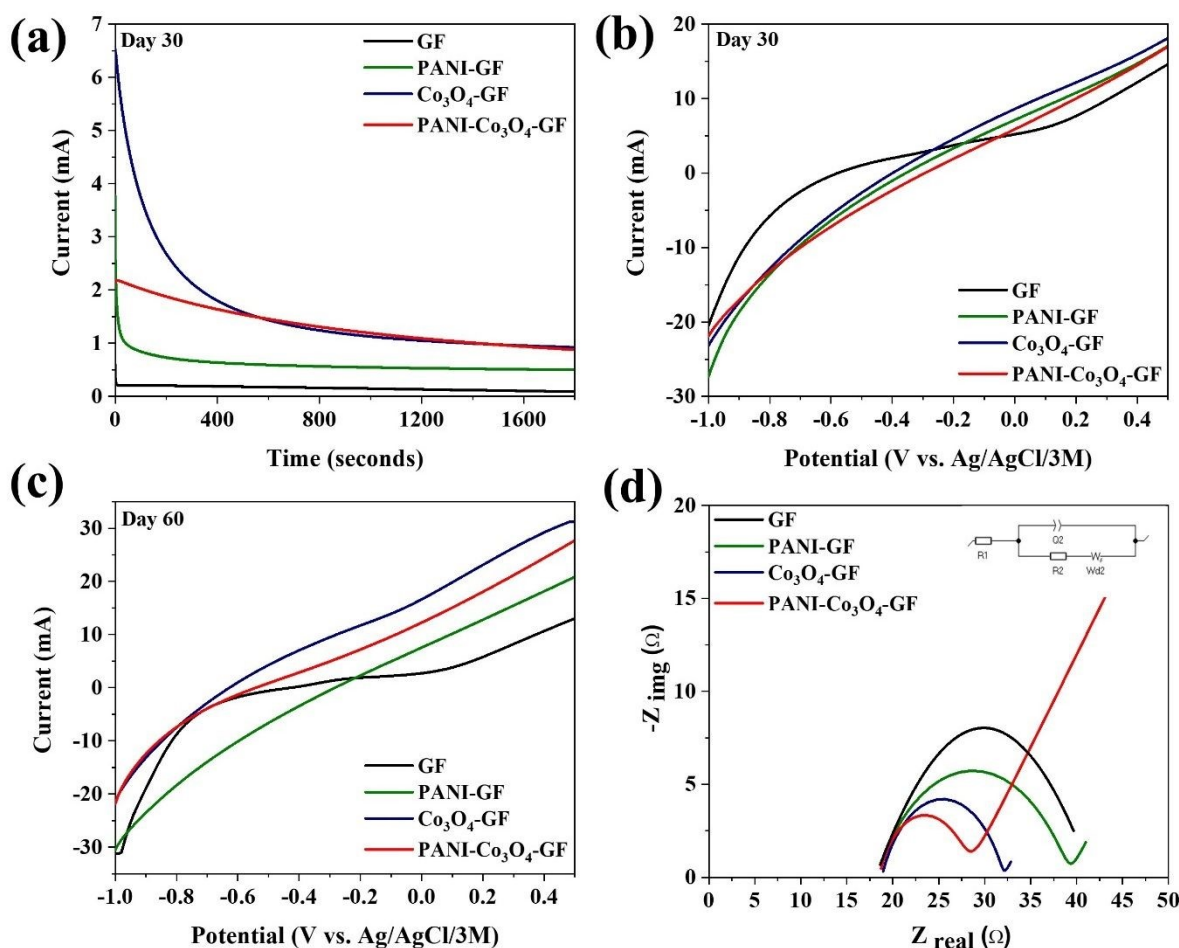
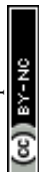


**Figure 6.** Electrochemical characterisation of the four anodes during operation in SMFCs. (a) CA tests at 250 V after 30 days of operation. (b and c) LSV scans at the scan rate  $0.01 \text{ V s}^{-1}$  after 30 and 60 days of operation. (d) EIS spectra of the anodes operated in SMFCs after four months of operation. Data in a, b and c are the averages of three replicates with a maximum standard deviation of  $\pm 3.1 \text{ mA}$ ,  $\pm 2.7 \text{ mA}$ ,  $\pm 1.5 \text{ mA}$  and  $\pm 1.8 \text{ mA}$ , respectively, for GF, PANI-GF,  $\text{Co}_3\text{O}_4$ -GF, and PANI- $\text{Co}_3\text{O}_4$ -GF.

CA analysis was conducted to measure the current produced as a function of anode modifications (**Figure 6a**). The potential used in the CA tests was selected on the basis of the closed-circuit potential against the highest power output of PANI- $\text{Co}_3\text{O}_4$ -GF from the polarization test conducted on day 7 of operation (measured as 246.7 mV, **Table S2**). As shown in **Figure 6a**, a sharp drop in current was recorded, possibly due to the charging effect <sup>75</sup>, followed by a slow decrease rate.  $\text{Co}_3\text{O}_4$ -GF was characterized by the highest drop in the current of 5.6 mA, followed by PANI-GF (3.3 mA), PANI- $\text{Co}_3\text{O}_4$ -GF (1.3 mA), and GF (0.5 mA). Although GF exhibits the lowest current drop, the great value of the retention rate, which is a measure of the electrode durability, for PANI- $\text{Co}_3\text{O}_4$ -GF (41.07%) compared to the other electrodes, suggests that GF functionalization with cobalt oxide and PANI leads to material better suitable for long-term applications <sup>76</sup>. Among the several types of anodes tested, PANI- $\text{Co}_3\text{O}_4$ -GF also records the highest current:  $0.88 \pm 14.5 \text{ mA}$  (**Table 2**). LSV studies further confirm the better performance of PANI- $\text{Co}_3\text{O}_4$ -GF (**Figure 6b and 6c**). At a potential of 0.48 V, the absolute value of the limiting current increased by a factor of 1.6, compared to 30 days of operation, reaching the value  $27.07 \pm 5.9 \text{ mA}$  for PANI- $\text{Co}_3\text{O}_4$ -GF after 60 days of operation. While,  $\text{Co}_3\text{O}_4$ -GF, PANI-GF, and GF recorded current of  $31.91 \pm 12.4 \text{ mA}$ ,  $20.38 \pm 9.3 \text{ mA}$ ,  $12.65 \pm 2.8 \text{ mA}$  on day 60 compared to respectively  $17.67 \pm 18.6 \text{ mA}$ ,  $16.61 \pm 8.9 \text{ mA}$ , and  $14.17 \pm 4.3 \text{ mA}$ , on day 30.

**Table 2.** Chronoamperometric values for the anodes (data refer to 3 replicates).

Anode material	current at 0 sec ( $i_0$ ) mA	current at 1800 sec ( $i_{1800}$ ) Ma	( $i_{1800}$ )/ ( $i_0$ )	Retention rate ( $i_{1800} \times 100$ )/ $i_0$ %
PANI- $\text{Co}_3\text{O}_4$ -GF	$2.13 \pm 16.4$	$0.88 \pm 14.5$	$0.4131 \pm 0.9$	41.31
PANI-GF	$3.76 \pm 23.8$	$0.50 \pm 6.2$	$0.1329 \pm 0.3$	13.26



Co <sub>3</sub> O <sub>4</sub> -GF	6.52 ± 36.4	0.9 ± 19.4	0.1411 ± 0.5	14.11
GF	0.59 ± 9.6	0.09 ± 3.6	0.1525 ± 0.4	15.25

As shown in **Figure 6d**, after 4 months of operation in the SMFCs, both the ohmic and charge transfer resistance changed significantly for each electrode. The increase in the ohmic resistance is a consequence of testing the anodes in soil rather than PBS. The solution resistance ( $R_1$ ) for GF, PANI-GF, Co<sub>3</sub>O<sub>4</sub>-GF, and PANI-Co<sub>3</sub>O<sub>4</sub>-GF was recorded as 18.64  $\Omega$ , 18.18  $\Omega$ , 18.95  $\Omega$ , and 18.72  $\Omega$ , respectively. The charge transfer resistance ( $R_2$ ) was the highest for GF, followed by PANI-GF, Co<sub>3</sub>O<sub>4</sub>-GF and PANI-Co<sub>3</sub>O<sub>4</sub>-GF (**Table 3**), implying the energy barrier for redox reaction was the lowest for PANI-Co<sub>3</sub>O<sub>4</sub>-GF<sup>77</sup>. The substitution of O ions in Co<sub>3</sub>O<sub>4</sub> and anions in PANI offers conducting holes, electron holes, and free electrons allowing the PANI chain to develop potential gradient and consequently promote charge transfer to lower the internal resistance barrier for redox reaction<sup>78</sup>. This improvement in the catalytic activity and electrode capacitance suggests high active site density/defects on the electrode surface substantially improves the electron transfer in SMFCs<sup>79</sup>. The reaction kinetics of the pristine GF enriched with biofilm is mainly controlled by charge transfer resistance; on the other hand, PANI-GF, Co<sub>3</sub>O<sub>4</sub>-GF, and PANI-Co<sub>3</sub>O<sub>4</sub>-GF show a combination of charge transfer resistance and pseudo capacitive property<sup>80</sup>. The CV and EIS spectra for the anodes before and after operation, and therefore biofilm growth onto the electrode surface, suggest that the redox active species within the biofilms have a positive effect on the extracellular electron transfer between the biofilms and the electrode surface.

**Table 3.** Resistances from EIS tests of the several anode electrodes before use and after 4 months operation in SMFC.

Anode	In 50 mM PBS solution		In SMFC (after 4 months)	
	Solution resistance ( $\Omega$ )	Charge transfer resistance ( $\Omega$ )	Solution resistance ( $\Omega$ )	Charge transfer resistance ( $\Omega$ )
GF	11.05	11.93	18.64	22.03
PANI-GF	13.38	18.92	18.18	21.04
Co <sub>3</sub> O <sub>4</sub> -GF	11.54	12.88	18.79	13.25

PANI-Co <sub>3</sub> O <sub>4</sub> -GF	13.54	12.01	18.52	9.58
---	-------	-------	-------	------

### 3.3. Measurement of the performance of anode composites in SMFCs

**Figure S2 and Figure S3** show the evolution of the anodic potential over time in SMFCs operated under closed-circuit potentials. After 60 s of operation, the anode potential for PANI-Co<sub>3</sub>O<sub>4</sub>-GF drops from +312 mV to a stable potential of around -478 mV, while the Co<sub>3</sub>O<sub>4</sub>-GF anode recorded -406 mV, followed by PANI-GF at -363 mV and GF at -305 mV. Among the several anodes, PANI-Co<sub>3</sub>O<sub>4</sub>-GF attains the negative potential in the shortest time (day 24), suggesting early biofilm formation and superior compatibility of the composite for biofilm enrichment <sup>79</sup>. Since, as expected, the performance of the cathode was similar in all devices tested (see polarisation curves of the cathode in **Figure S4 (a)**), the performance difference in the several SMFCs can be attributed to the anode. PANI-Co<sub>3</sub>O<sub>4</sub>-GF showed the highest potential (in absolute value) amongst the several types of anode tested, which favours the oxidation reactions at anode with low charge transfer resistance **Figure S4 (b)** <sup>80</sup>.





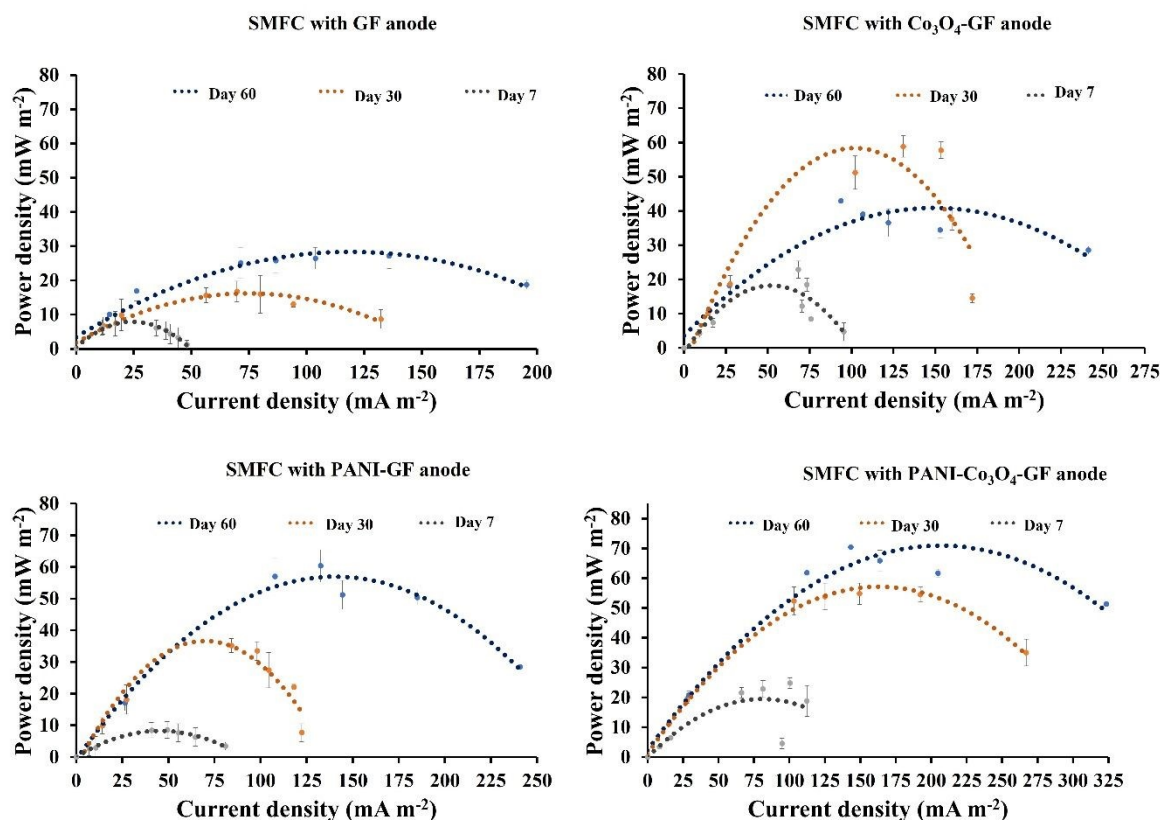
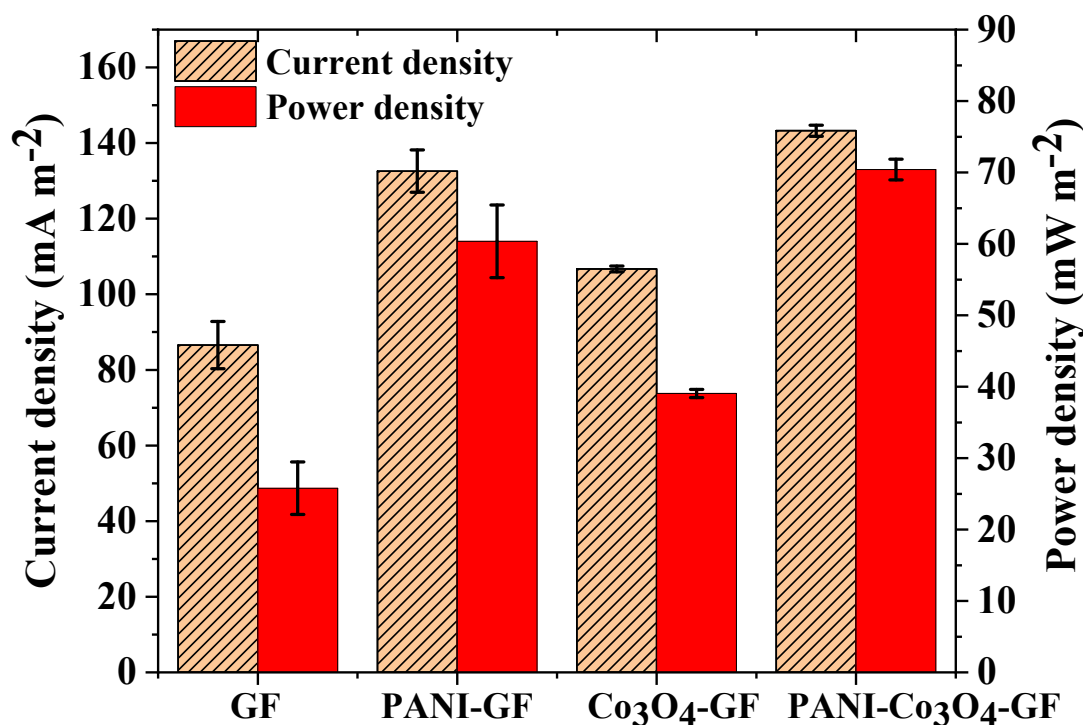


**Figure 7** Comparison of power curves obtained with the SMFCs implementing the different types of anode materials at 7, 30 and 60 days of operation. Error bars refer to three replicates.

The power curves confirm the outperformance of the SMFCs with the PANI-Co<sub>3</sub>O<sub>4</sub>-GF anode. As shown in **Figure 7**, except for the SMFC implementing the Co<sub>3</sub>O<sub>4</sub>-GF anode, the peak power density and the peak current density increased with time (**Table S2**). In the case of the SMFC implementing the Co<sub>3</sub>O<sub>4</sub>-GF anode, after a 2.58 times increase in the power output after 30 days of operation, after 60 days of operation the increase with respect to day 7 was only 1.88 times. Contact angle measurements and CV studies confirm that Co<sub>3</sub>O<sub>4</sub>-GF exhibits low hydrophobicity and electrochemical surface area, leading to better performance than plain GF. Nonetheless, the decrease in performance after 60 days of operation suggests poor stability of the electrode. PANI coating enhances the performance of plain GF, as the SMFC implementing the PANI-GF anode generated a peak power density 2.59 times higher than the SMFC with plain GF anode after 60 days of operation. Moreover, PANI also contributes to stabilising Co<sub>3</sub>O<sub>4</sub> on GF, as shown by the sustained greater performance of the SMFC implementing the PANI-Co<sub>3</sub>O<sub>4</sub>-GF anode.

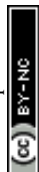






**Figure 8.** Comparison of power and current profile of anodes at 700  $\Omega$  on day 60. Error bars refer to three replicates.

The SMFC with the PANI-Co<sub>3</sub>O<sub>4</sub>-GF anode generated the maximum power density, with a peak value of  $70.4 \pm 1.4 \text{ mW m}^{-2}$ , corresponding to a current density of  $143.2 \pm 1.4 \text{ mA m}^{-2}$ . This corresponds to a 63.81% increase for the SMFC with the Co<sub>3</sub>O<sub>4</sub>-GF anode ( $42.9 \pm 0.7 \text{ mW m}^{-2}$ ), a 16.62% increase over the SMFC with PANI-GF ( $60.4 \pm 5.1 \text{ mW m}^{-2}$ ), and a 158.69% increase for the case of the SMFC with GF anode ( $27.2 \pm 3.7 \text{ mW m}^{-2}$ ) (**Figure 8**). The high redox potential of PANI-Co<sub>3</sub>O<sub>4</sub>-GF favours the electron movement along the microbial transfer chains to the high potential anode, rendering them compatible for microbial adhesion<sup>81</sup>. The interweaving of polyaniline on Co<sub>3</sub>O<sub>4</sub>-GF resulted in better power performance, unlike Co<sub>3</sub>O<sub>4</sub>-GF anode-based SMFC, where limited electron diffusion from biofilm to Co<sub>3</sub>O<sub>4</sub>-GF electrode suppressed the performance of the system with time.



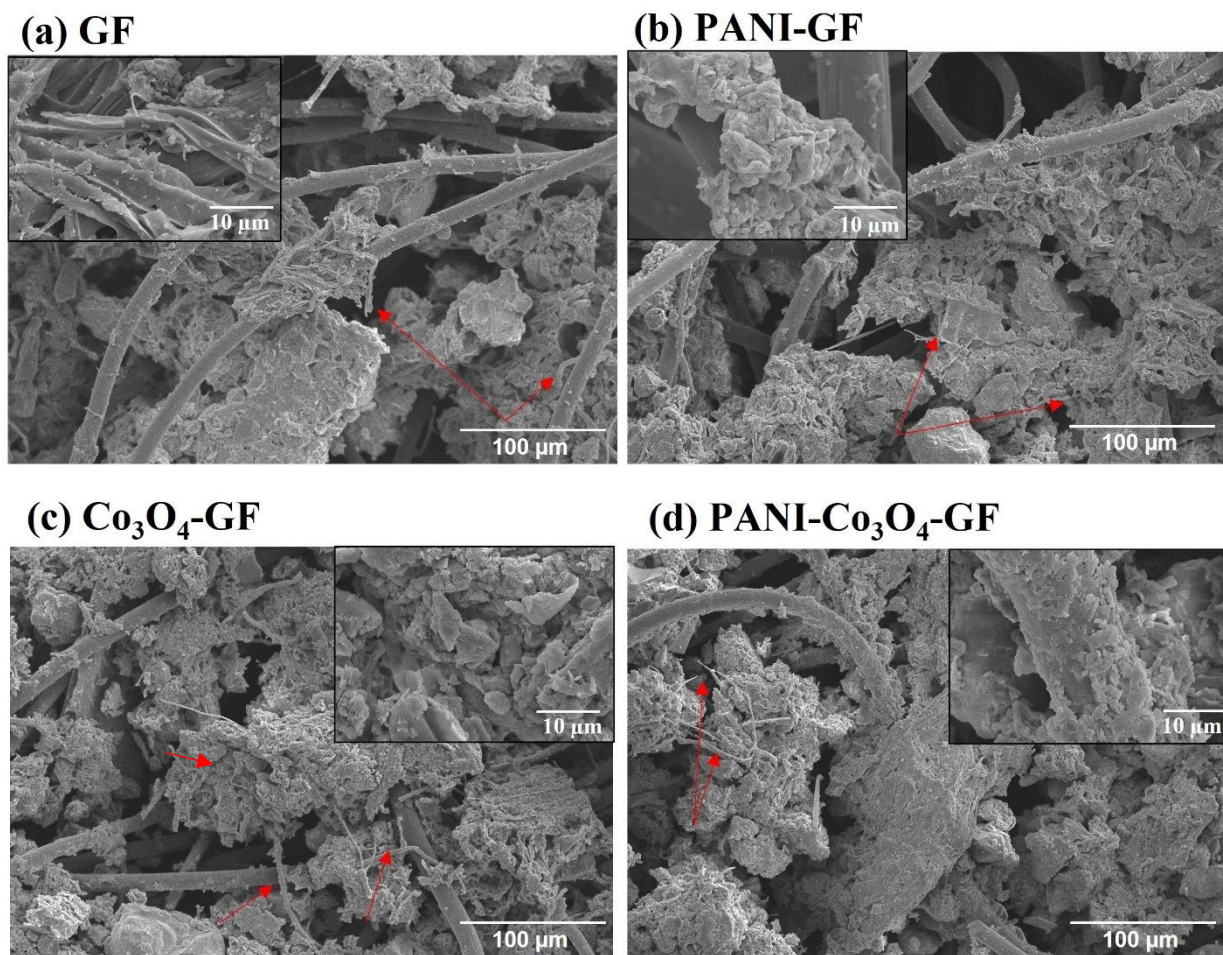


**Figure 9.** SEM images of inoculated GF (a), PANI-GF (b),  $\text{Co}_3\text{O}_4$ -GF (c) PANI- $\text{Co}_3\text{O}_4$ -GF (d) electrodes (at 10 kV, magnification: 300). Red arrows in the images indicate filamentous assemblies.

‘The biofilms growth on anodes plays a crucial role in SMFCs for converting the chemical energy of the organics in soil to energy. The morphology of the biofilm developed onto the anode surface was investigated by SEM. As shown in **Figure 9 (a-b)**, the cell density was low on the surface of the GF and PANI-GF electrodes, while a more uniform biofilm coverage was observed in the case of  $\text{Co}_3\text{O}_4$ -GF (**Figure 9c**) and PANI- $\text{Co}_3\text{O}_4$ -GF (**Figure 9d**). This result supports the hypothesis that  $\text{Co}_3\text{O}_4$  nanoparticles improve the electrode biocompatibility and microbial adhesion<sup>80</sup>. The SEM images (Figure 9c and 9d) reveal a highly dense biofilm, with a wide range of shape and size of microbes and filamentous microorganism assemblies colonizing the electrodes (marked with red arrows). The presence of such filaments is beneficial for connecting the felt fibres, thus enhancing the charge transfer between the biofilm and the electrode interface<sup>84</sup>. Dense and

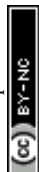


uniformly covered fibres of PANI-Co<sub>3</sub>O<sub>4</sub>-GF could be attributed to the roughness, decreased hydrophobicity, and porous surface of the electrode <sup>85</sup>. These results also suggest that the conductive-nanowire like filamentous microorganism in the biofilm were well embedded in the composite matrix, boosting the extracellular electron transport in the SMFCs.

Further investigations, involving next generation sequencing, should be carry out in future work to assess if and how the functionalisation strategy proposed in this study influences the microbial composition of the anodic biofilm.'

#### 4. Conclusion

Soil microbial fuel cell has a great potential as a renewable energy harvesting technology as well as a self-powered bioremediation strategy. Performance depends on material and design of the electrodes implemented and, particularly for the case of the anode, electrode high specific surface area is key for a highly performing electroactive biofilm. In this study, graphite felt was functionalised with cobalt oxide and/or PANI to generate two different anode materials, Co<sub>3</sub>O<sub>4</sub>-GF and PANI-Co<sub>3</sub>O<sub>4</sub>-GF, tested for the first time in SMFCs. The performance of SMFCs implementing these anodes was compared, and benchmarked against two control SMFC devices, implementing a PANI functionalised GF anode (PANI-GF), to elucidate the effect of PANI on performance, and a plain GF anode. The highest power density was observed with the SMFC implementing the PANI-Co<sub>3</sub>O<sub>4</sub>-GF anode: with a peak power of 70 mW m<sup>-2</sup> after 60 days of operation. This value was 1.6 times higher than the case of Co<sub>3</sub>O<sub>4</sub>-GF anode, 1.3 times higher than the case of SMFC with PANI-GF anode, and 2.6 times higher than the case of GF anode. Indeed, initially (up to 30 days of operation) the SMFC with the Co<sub>3</sub>O<sub>4</sub>-GF anode showed the best performance, however the stability was poor; after 60 days of operation, the power density generated by the SMFC with the Co<sub>3</sub>O<sub>4</sub>-GF anode decreased by over 30% with respect to 30 days of operation, probably due to Co<sub>3</sub>O<sub>4</sub> leaching. These results suggest that PANI has an important role in stabilising the Co<sub>3</sub>O<sub>4</sub> nanostructure onto the GF electrode surface. PANI also favours the development of a functional electrochemical biofilm, as demonstrated by the performance enhancement of the SMFC with the PANI-GF anode with respect to the use of plain GF. While the cause for instability of the Co<sub>3</sub>O<sub>4</sub>-GF electrode must be better investigated, this study confirms



the benefits of implementing metal oxide-conductive polymer composite electrode materials as anode for better SMFC performance, and accordingly inspires future trends in the field.

### CRediT authorship contribution statement

**Simran Kaur Dhillon**: Conceptualization, investigation, methodology, electrochemical analysis, validation, data curation, writing-original draft, formal analysis. **Jakub Dziegielowski**: Conceptualization and writing-data interpretation. **Patit Paban Kundu**: Supervision, Writing-review, editing. **Mirella Di Lorenzo**: Supervision, conceptualization, data validation, and curation, writing-data interpretation and writing, funding securing.

### Funding sources

This work is part of the project GREENER that has received funding from the European Union's Horizon 2020 research and innovation programme under the grant agreement No 826312.

Simran Kaur Dhillon received funding from the Commonwealth spli-site PhD scholarship to carry out work at the University of Bath.

### Competing Interest Declaration

The authors declare no known competing financial interests.

### Acknowledgments

The authors thank: Ministry of Human Resource Development (MHRD), Govt. of India for funding Simran Kaur Dhillon's PhD scholarship at IIT Roorkee; Commonwealth spli-site PhD scholarship for funding Simran Kaur Dhillon's visit at the University of Bath; European Union's Horizon 2020 research and innovation programme for funding.

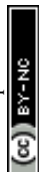
### References

- (1) Kumar, R.; Singh, L.; Zularisam, A. W.; Hai, F. I. Microbial Fuel Cell Is Emerging as a Versatile Technology: A Review on Its Possible Applications, Challenges and Strategies to Improve the Performances. *Int. J. Energy Res.* **2018**, *42* (2), 369–394. <https://doi.org/10.1002/er.3780>.
- (2) Bajracharya, S.; Sharma, M.; Mohanakrishna, G.; Dominguez Benneton, X.; Strik, D. P. B.





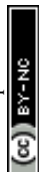
- T. B.; Sarma, P. M.; Pant, D. An Overview on Emerging Bioelectrochemical Systems (BESs): Technology for Sustainable Electricity, Waste Remediation, Resource Recovery, Chemical Production and Beyond. *Renew. Energy* **2016**, *98*, 153–170. <https://doi.org/10.1016/j.renene.2016.03.002>.
- (3) Dziegielowski, J.; Metcalfe, B.; Villegas-Guzman, P.; Martínez-Huitile, C. A.; Gorayeb, A.; Wenk, J.; Di Lorenzo, M. Development of a Functional Stack of Soil Microbial Fuel Cells to Power a Water Treatment Reactor: From the Lab to Field Trials in North East Brazil. *Appl. Energy* **2020**, *278* (August). <https://doi.org/10.1016/j.apenergy.2020.115680>.
  - (4) Casula, E.; Kim, B.; Chesson, H.; Di Lorenzo, M.; Mascia, M. Modelling the Influence of Soil Properties on Performance and Bioremediation Ability of a Pile of Soil Microbial Fuel Cells. *Electrochim. Acta* **2021**, *368*. <https://doi.org/10.1016/j.electacta.2020.137568>.
  - (5) Dunaj, S. J.; Vallino, J. J.; Hines, M. E.; Gay, M.; Kobyljanec, C.; Rooney-Varga, J. N. Relationships between Soil Organic Matter, Nutrients, Bacterial Community Structure, and the Performance of Microbial Fuel Cells. *Environ. Sci. Technol.* **2012**, *46* (3), 1914–1922. <https://doi.org/10.1021/es2032532>.
  - (6) Chicca, I.; Becarelli, S.; Di Gregorio, S. Microbial Involvement in the Bioremediation of Total Petroleum Hydrocarbon Polluted Soils: Challenges and Perspectives. *Environ. - MDPI* **2022**, *9* (4). <https://doi.org/10.3390/environments9040052>.
  - (7) Dziegielowski, J.; Bregu, G.; Hulse, L.; Di Lorenzo, M. Assessing the Effect of the Electrode Orientation on the Performance of Soil Microbial Fuel Cells. *E3S Web Conf.* **2022**, *334*, 08003. <https://doi.org/10.1051/e3sconf/202233408003>.
  - (8) Sun, Y.; Wei, J.; Liang, P.; Huang, X. Electricity Generation and Microbial Community Changes in Microbial Fuel Cells Packed with Different Anodic Materials. *Bioresour. Technol.* **2011**, *102* (23), 10886–10891. <https://doi.org/10.1016/j.biortech.2011.09.038>.
  - (9) Abbas, S. Z.; Rafatullah, M. Recent Advances in Soil Microbial Fuel Cells for Soil Contaminants Remediation. *Chemosphere* **2021**, *272*, 129691. <https://doi.org/10.1016/j.chemosphere.2021.129691>.
  - (10) Dhillon, S. K.; Kundu, P. P.; Jain, R. Catalytic Advancements in Carbonaceous Materials for Bio-Energy Generation in Microbial Fuel Cells: A Review. *Environ. Sci. Pollut. Res.* **2022**, No. 0123456789. <https://doi.org/10.1007/s11356-021-17529-9>.
  - (11) Liu, H.; Ramnarayanan, R.; Logan, B. E. Production of Electricity during Wastewater



- Treatment Using a Single Chamber Microbial Fuel Cell. *Environ. Sci. Technol.* **2004**, *38* (7), 2281–2285. <https://doi.org/10.1021/es034923g>.
- (12) Nitisoravut, R.; Thanh, C. N. D.; Regmi, R. Microbial Fuel Cells: Advances in Electrode Modifications for Improvement of System Performance. *Int. J. Green Energy* **2017**, *14* (8), 712–723. <https://doi.org/10.1080/15435075.2017.1326049>.
- (13) Erable, B.; Byrne, N.; Etcheverry, L.; Achouak, W.; Bergel, A. Single Medium Microbial Fuel Cell: Stainless Steel and Graphite Electrode Materials Select Bacterial Communities Resulting in Opposite Electrocatalytic Activities. *Int. J. Hydrogen Energy* **2017**, *42* (41), 26059–26067. <https://doi.org/10.1016/j.ijhydene.2017.08.178>.
- (14) Santoro, C.; Arbizzani, C.; Erable, B.; Ieropoulos, I. Microbial Fuel Cells: From Fundamentals to Applications. A Review. *J. Power Sources* **2017**, *356*, 225–244. <https://doi.org/10.1016/j.jpowsour.2017.03.109>.
- (15) Chen, S.; Tang, J.; Fu, L.; Yuan, Y.; Zhou, S. Biochar Improves Sediment Microbial Fuel Cell Performance in Low Conductivity Freshwater Sediment. *J. Soils Sediments* **2016**, *16* (9), 2326–2334. <https://doi.org/10.1007/s11368-016-1452-z>.
- (16) Li, X.; Wang, X.; Zhao, Q.; Wan, L.; Li, Y.; Zhou, Q. Carbon Fiber Enhanced Bioelectricity Generation in Soil Microbial Fuel Cells. *Biosens. Bioelectron.* **2016**, *85*, 135–141. <https://doi.org/10.1016/j.bios.2016.05.001>.
- (17) Pinto, D.; Coradin, T.; Laberty-Robert, C. Effect of Anode Polarization on Biofilm Formation and Electron Transfer in *Shewanella Oneidensis*/Graphite Felt Microbial Fuel Cells. *Bioelectrochemistry* **2018**, *120*, 1–9. <https://doi.org/10.1016/j.bioelechem.2017.10.008>.
- (18) Yu, B.; Feng, L.; He, Y.; Yang, L.; Xun, Y. Effects of Anode Materials on the Performance and Anode Microbial Community of Soil Microbial Fuel Cell. *J. Hazard. Mater.* **2021**, *401* (April 2020), 123394. <https://doi.org/10.1016/j.jhazmat.2020.123394>.
- (19) Yang, W.; Wang, X.; Son, M.; Logan, B. E. Simultaneously Enhancing Power Density and Coulombic Efficiency with a Hydrophobic Fe–N4/Activated Carbon Air Cathode for Microbial Fuel Cells. *J. Power Sources* **2020**, *465* (February), 228264. <https://doi.org/10.1016/j.jpowsour.2020.228264>.
- (20) Afkhami, A.; Madrakian, T.; Karimi, Z. The Effect of Acid Treatment of Carbon Cloth on the Adsorption of Nitrite and Nitrate Ions. *J. Hazard. Mater.* **2007**, *144* (1–2), 427–431.



- <https://doi.org/10.1016/j.jhazmat.2006.10.062>.
- (21) Dhillon, S. K.; Chaturvedi, A.; Gupta, D.; Nagaiah, T. C.; Kundu, P. P. Copper Nanoparticles Embedded in Polyaniline Derived Nitrogen-Doped Carbon as Electrocatalyst for Bio-Energy Generation in Microbial Fuel Cells. *Environ. Sci. Pollut. Res.* **2022**. <https://doi.org/10.1007/s11356-022-21437-x>.
- (22) Yu, B.; Li, Y.; Feng, L. Enhancing the Performance of Soil Microbial Fuel Cells by Using a Bentonite-Fe and Fe<sub>3</sub>O<sub>4</sub> Modified Anode. *J. Hazard. Mater.* **2019**, 377 (March), 70–77. <https://doi.org/10.1016/j.jhazmat.2019.05.052>.
- (23) Xu, H.; Quan, X.; Xiao, Z.; Chen, L. Effect of Anodes Decoration with Metal and Metal Oxides Nanoparticles on Pharmaceutically Active Compounds Removal and Power Generation in Microbial Fuel Cells. *Chem. Eng. J.* **2018**, 335 (November 2017), 539–547. <https://doi.org/10.1016/j.cej.2017.10.159>.
- (24) Huang, Q.; Zhou, P.; Yang, H.; Zhu, L.; Wu, H. In Situ Generation of Inverse Spinel CoFe<sub>2</sub>O<sub>4</sub> Nanoparticles onto Nitrogen-Doped Activated Carbon for an Effective Cathode Electrocatalyst of Microbial Fuel Cells. *Chem. Eng. J.* **2017**, 325, 466–473. <https://doi.org/10.1016/j.cej.2017.05.079>.
- (25) Wang, X.; Liu, W.; Fu, H.; Yi, X. H.; Wang, P.; Zhao, C.; Wang, C. C.; Zheng, W. Simultaneous Cr(VI) Reduction and Cr(III) Removal of Bifunctional MOF/Titanate Nanotube Composites. *Environ. Pollut.* **2019**, 249, 502–511. <https://doi.org/10.1016/j.envpol.2019.03.096>.
- (26) Veeramani, V.; Rajangam, K.; Nagendran, J. Performance of Cobalt Oxide/Carbon Cloth Composite Electrode in Energy Generation from Dairy Wastewater Using Microbial Fuel Cells. *Sustain. Environ. Res.* **2020**, 30 (1), 0–7. <https://doi.org/10.1186/s42834-020-00058-4>.
- (27) Kasem, E. T.; Tsujiguchi, T.; Nakagawa, N. Effect of Metal Modification to Carbon Paper Anodes on the Performance of Yeast-Based Microbial Fuel Cells Part II: In the Case with Exogenous Mediator, Methylene Blue. *Key Eng. Mater.* **2013**, 534 (August 2014), 82–87. <https://doi.org/10.4028/www.scientific.net/KEM.534.82>.
- (28) Li, B.; Logan, B. E. Bacterial Adhesion to Glass and Metal-Oxide Surfaces. *Colloids Surfaces B Biointerfaces* **2004**, 36 (2), 81–90. <https://doi.org/10.1016/j.colsurfb.2004.05.006>.

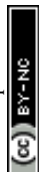




- (29) Vagin, M.; Gueskine, V.; Mitraka, E.; Wang, S.; Singh, A.; Zozoulenko, I.; Berggren, M.; Fabiano, S.; Crispin, X. Negatively-Doped Conducting Polymers for Oxygen Reduction Reaction. *Adv. Energy Mater.* **2021**, *11* (3), 1–8. <https://doi.org/10.1002/aenm.202002664>.
- (30) Dutta, K.; Kundu, P. P. A Review on Aromatic Conducting Polymers-Based Catalyst Supporting Matrices for Application in Microbial Fuel Cells. *Polym. Rev.* **2014**, *54* (3), 401–435. <https://doi.org/10.1080/15583724.2014.881372>.
- (31) Li, C.; Zhang, L.; Ding, L.; Ren, H.; Cui, H. Effect of Conductive Polymers Coated Anode on the Performance of Microbial Fuel Cells (MFCs) and Its Biodiversity Analysis. *Biosens. Bioelectron.* **2011**, *26* (10), 4169–4176. <https://doi.org/10.1016/j.bios.2011.04.018>.
- (32) Kaur Dhillon, S.; Kundu, P. P. Polyaniline Interweaved Iron Embedded in Urea-Formaldehyde Resin-Based Carbon as a Cost-Effective Catalyst for Power Generation in Microbial Fuel Cell. *Chem. Eng. J.* **2021**, No. August, 133341. <https://doi.org/10.1016/j.cej.2021.133341>.
- (33) Dhillon, S. K.; Kundu, P. P. Development of Polypyrrole Nanotube Coated with Chitosan and Nickel Oxide as a Biocompatible Anode to Enhance the Power Generation in Microbial Fuel Cell. *J. Power Sources* **2022**, *539* (May), 231595. <https://doi.org/10.1016/j.jpowsour.2022.231595>.
- (34) Mohamed, H. O.; Abdelkareem, M. A.; Obaid, M.; Chae, S. H.; Park, M.; Kim, H. Y.; Barakat, N. A. M. Cobalt Oxides-Sheathed Cobalt Nano Flakes to Improve Surface Properties of Carbonaceous Electrodes Utilized in Microbial Fuel Cells. *Chem. Eng. J.* **2017**, *326*, 497–506. <https://doi.org/10.1016/j.cej.2017.05.166>.
- (35) Song, R. Bin; Yan, K.; Lin, Z. Q.; Chye Loo, J. S.; Pan, L. J.; Zhang, Q.; Zhang, J. R.; Zhu, J. J. Inkjet-Printed Porous Polyaniline Gel as an Efficient Anode for Microbial Fuel Cells. *J. Mater. Chem. A* **2016**, *4* (38), 14555–14559. <https://doi.org/10.1039/c6ta05770e>.
- (36) Zamani, P.; Higgins, D.; Hassan, F.; Jiang, G.; Wu, J.; Abureden, S.; Chen, Z. Electrospun Iron-Polyaniline-Polyacrylonitrile Derived Nanofibers as Non-Precious Oxygen Reduction Reaction Catalysts for PEM Fuel Cells. *Electrochim. Acta* **2014**, *139*, 111–116. <https://doi.org/10.1016/j.electacta.2014.07.007>.
- (37) Champigneux, P.; Renault-Sentenac, C.; Bourrier, D.; Rossi, C.; Delia, M. L.; Bergel, A. Effect of Surface Roughness, Porosity and Roughened Micro-Pillar Structures on the Early Formation of Microbial Anodes. *Bioelectrochemistry* **2019**, *128*, 17–29.



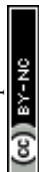
- <https://doi.org/10.1016/j.bioelechem.2019.03.002>.
- (38) Zou, L.; Qiao, Y.; Zhong, C.; Li, C. M. Enabling Fast Electron Transfer through Both Bacterial Outer-Membrane Redox Centers and Endogenous Electron Mediators by Polyaniline Hybridized Large-Mesoporous Carbon Anode for High-Performance Microbial Fuel Cells. *Electrochim. Acta* **2017**, *229*, 31–38. <https://doi.org/10.1016/j.electacta.2017.01.081>.
- (39) Yong, Y. C.; Dong, X. C.; Chan-Park, M. B.; Song, H.; Chen, P. Macroporous and Monolithic Anode Based on Polyaniline Hybridized Three-Dimensional Graphene for High-Performance Microbial Fuel Cells. *ACS Nano* **2012**, *6* (3), 2394–2400. <https://doi.org/10.1021/nn204656d>.
- (40) Zhao, C.; Gai, P.; Liu, C.; Wang, X.; Xu, H.; Zhang, J.; Zhu, J. J. Polyaniline Networks Grown on Graphene Nanoribbons-Coated Carbon Paper with a Synergistic Effect for High-Performance Microbial Fuel Cells. *J. Mater. Chem. A* **2013**, *1* (40), 12587–12594. <https://doi.org/10.1039/c3ta12947k>.
- (41) Lin, X.; Shang, Y.; Li, L.; Yu, A. Sea-Urchin-like Cobalt Oxide Grown on Nickel Foam as a Carbon-Free Electrode for Lithium-Oxygen Batteries. *ACS Sustain. Chem. Eng.* **2015**, *3* (5), 903–908. <https://doi.org/10.1021/acssuschemeng.5b00012>.
- (42) Narayanasamy, S.; Jayaprakash, J. Carbon Cloth/Nickel Cobaltite (NiCo<sub>2</sub>O<sub>4</sub>)/Polyaniline (PANI) Composite Electrodes: Preparation, Characterization, and Application in Microbial Fuel Cells. *Fuel* **2021**, *301* (May). <https://doi.org/10.1016/j.fuel.2021.121016>.
- (43) Su, F.; Wang, F.; Zhang, C.; Lu, T.; Zhang, S.; Zhang, R.; Qi, X.; Liu, P. Ameliorating Substance Accessibility for Microorganisms to Amplify Toluene Degradation and Power Generation of Microbial Fuel Cell by Using Activated Carbon Anode. *J. Clean. Prod.* **2022**, 377. <https://doi.org/10.1016/j.jclepro.2022.134481>.
- (44) Casula, E.; Kim, B.; Chesson, H.; Di Lorenzo, M.; Mascia, M. Modelling the Influence of Soil Properties on Performance and Bioremediation Ability of a Pile of Soil Microbial Fuel Cells. *Electrochim. Acta* **2021**, 368. <https://doi.org/10.1016/j.electacta.2020.137568>.
- (45) Dujearic-Stephane, K.; Gupta, M.; Kumar, A.; Sharma, V.; Pandit, S.; Bocchetta, P.; Kumar, Y. The Effect of Modifications of Activated Carbon Materials on the Capacitive Performance: Surface, Microstructure, and Wettability. *J. Compos. Sci.* **2021**, *5* (3). <https://doi.org/10.3390/jcs5030066>.



- (46) Gao, S.; Mi, H.; Li, Z.; Ji, C.; Sun, L.; Yu, C.; Qiu, J. Porous Polyaniline Arrays Oriented on Functionalized Carbon Cloth as Binder-Free Electrode for Flexible Supercapacitors. *J. Electroanal. Chem.* **2019**, *848*, 113348. <https://doi.org/10.1016/j.jelechem.2019.113348>.
- (47) Zhou, J.; Zhang, H.; Zuo, T.; Jia, Q.; Wang, L.; Tian, Y.; Gong, L.; Zhou, Y.; Wang, J. Enhanced Copper-Containing Wastewater Treatment with MnO<sub>2</sub>/CNTs Modified Anode Microbial Fuel Cell. *Process Saf. Environ. Prot.* **2022**, *159*, 157–167. <https://doi.org/10.1016/j.psep.2021.12.060>.
- (48) Lu, J.; Ayele, B. A.; Liu, X.; Chen, Q. Electrochemical Removal of RRX-3B in Residual Dyeing Liquid with Typical Engineered Carbonaceous Cathodes. *J. Environ. Manage.* **2021**, *280* (August 2020), 111669. <https://doi.org/10.1016/j.jenvman.2020.111669>.
- (49) Medium, A.; Ni, M.; Synergism, C. O. C.; Matthews, T.; Dolla, T. H.; Gwebu, S. S.; Mashola, T. A.; Dlamini, L. T.; Carleschi, E.; Ndungu, P.; Maxakato, N. W. Mn-Ni-Co-O Spinel Oxides towards Oxygen Reduction Reaction in Alkaline Medium: Mn<sub>0.5</sub>Ni<sub>0.5</sub>Co<sub>2</sub>O<sub>4</sub>/C Synergism and Cooperation. *Catalysts* **2021**, *Catalysts*.
- (50) Xu, H.; Wu, J. X.; Chen, Y.; Zhang, J. L.; Zhang, B. Q. Facile Synthesis of Polyaniline/NiCo<sub>2</sub>O<sub>4</sub> Nanocomposites with Enhanced Electrochemical Properties for Supercapacitors. *Ionics (Kiel)*. **2015**, *21* (9), 2615–2622. <https://doi.org/10.1007/s11581-015-1441-z>.
- (51) Ilkiv, B.; Petrovska, S.; Sergiienko, R.; Foya, O.; Ilkiv, O.; Shibata, E.; Nakamura, T.; Zaulychnyy, Y. Electronic Structure of Hollow Graphitic Carbon Nanoparticles Fabricated from Acetylene Carbon Black. *Fullerenes Nanotub. Carbon Nanostructures* **2015**, *23* (5), 449–454. <https://doi.org/10.1080/1536383X.2014.885957>.
- (52) Zhang, Z.; Xi, J.; Zhou, H.; Qiu, X. KOH Etched Graphite Felt with Improved Wettability and Activity for Vanadium Flow Batteries. *Electrochim. Acta* **2016**, *218*, 15–23. <https://doi.org/10.1016/j.electacta.2016.09.099>.
- (53) He, X.; Gao, B.; Wang, G.; Wei, J.; Zhao, C. A New Nanocomposite: Carbon Cloth Based Polyaniline for Anelectrochemical Supercapacitor. *Electrochim. Acta* **2013**, *111*, 210–215. <https://doi.org/10.1016/j.electacta.2013.07.226>.
- (54) Ahirrao, D. J.; Pal, A. K.; Singh, V.; Jha, N. Nanostructured Porous Polyaniline (PANI) Coated Carbon Cloth (CC) as Electrodes for Flexible Supercapacitor Device. *J. Mater. Sci. Technol.* **2021**, *88*, 168–182. <https://doi.org/10.1016/j.jmst.2021.01.075>.



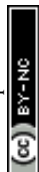
- (55) Casado, U. M.; Aranguren, M. I.; Marcovich, N. E. Preparation and Characterization of Conductive Nanostructured Particles Based on Polyaniline and Cellulose Nanofibers. *Ultrason. Sonochem.* **2014**, *21* (5), 1641–1648. <https://doi.org/10.1016/j.ultsonch.2014.03.012>.
- (56) Mu, J.-C.; Wang, E.-Q.; Zhang, Y.-L.; Zhang, L.-P. A Novel and Green Synthesis of Mixed Phase CoO@Co<sub>3</sub>O<sub>4</sub>@C Anode Material for Lithium Ion Batteries. *J. Nanosci. Nanotechnol.* **2019**, *19* (12), 7819–7825. <https://doi.org/10.1166/jnn.2019.16744>.
- (57) Montazerzohori, M.; Masoudiasl, A.; Farokhiyani, S.; Joohari, S.; McArdle, P. Sonochemical Synthesis of a New Cobalt(II) Complex: Crystal Structure, Thermal Behavior, Hirshfeld Surface Analysis and Its Usage as Precursor for Preparation of CoO/Co<sub>3</sub>O<sub>4</sub> Nanoparticles. *Ultrason. Sonochem.* **2017**, *38*, 134–144. <https://doi.org/10.1016/j.ultsonch.2017.03.017>.
- (58) Rethinasabapathy, M.; Vilian, A. T. E.; Hwang, S. K.; Kang, S. M.; Cho, Y.; Han, Y. K.; Rhee, J. K.; Huh, Y. S. Cobalt Ferrite Microspheres as a Biocompatible Anode for Higher Power Generation in Microbial Fuel Cells. *J. Power Sources* **2021**, *483* (November 2020), 229170. <https://doi.org/10.1016/j.jpowsour.2020.229170>.
- (59) Mashao, G.; Modibane, K. D.; Mdluli, S. B.; Iwuoha\*, E. I.; Hato, M. J.; Makgopa, K.; Molapo, K. M. Polyaniline-Cobalt Benzimidazolate Zeolitic Metal-Organic Framework Composite Material for Electrochemical Hydrogen Gas Sensing. *Electrocatalysis* **2019**, *10* (4), 406–419. <https://doi.org/10.1007/s12678-019-00529-2>.
- (60) Yamashita, T.; Yokoyama, H. Molybdenum Anode: A Novel Electrode for Enhanced Power Generation in Microbial Fuel Cells, Identified via Extensive Screening of Metal Electrodes. *Biotechnol. Biofuels* **2018**, *11* (1), 1–13. <https://doi.org/10.1186/s13068-018-1046-7>.
- (61) Yin, T.; Lin, Z.; Su, L.; Yuan, C.; Fu, D. Preparation of Vertically Oriented TiO<sub>2</sub> Nanosheets Modified Carbon Paper Electrode and Its Enhancement to the Performance of MFCs. *ACS Appl. Mater. Interfaces* **2015**, *7* (1), 400–408. <https://doi.org/10.1021/am506360x>.
- (62) Farahmand Habibi, M.; Arvand, M.; Sohrabnezhad, S. Boosting Bioelectricity Generation in Microbial Fuel Cells Using Metal@metal Oxides/Nitrogen-Doped Carbon Quantum Dots. *Energy* **2021**, *223*, 120103. <https://doi.org/10.1016/j.energy.2021.120103>.
- (63) Jiang, H. R.; Zeng, Y. K.; Wu, M. C.; Shyy, W.; Zhao, T. S. A Uniformly Distributed



- Bismuth Nanoparticle-Modified Carbon Cloth Electrode for Vanadium Redox Flow Batteries. *Appl. Energy* **2019**, *240* (July 2018), 226–235. <https://doi.org/10.1016/j.apenergy.2019.02.051>.
- (64) Ali, A.; Hantanasirisakul, K.; Abdala, A.; Urbankowski, P.; Zhao, M. Q.; Anasori, B.; Gogotsi, Y.; Aïssa, B.; Mahmoud, K. A. Effect of Synthesis on Performance of MXene/Iron Oxide Anode Material for Lithium-Ion Batteries. *Langmuir* **2018**, *34* (38), 11325–11334. <https://doi.org/10.1021/acs.langmuir.8b01953>.
- (65) Han, T. H.; Parveen, N.; Shim, J. H.; Nguyen, A. T. N.; Mahato, N.; Cho, M. H. Ternary Composite of Polyaniline Graphene and TiO<sub>2</sub> as a Bifunctional Catalyst to Enhance the Performance of Both the Bioanode and Cathode of a Microbial Fuel Cell. *Ind. Eng. Chem. Res.* **2018**, *57* (19), 6705–6713. <https://doi.org/10.1021/acs.iecr.7b05314>.
- (66) Lei, C.; Han, F.; Li, D.; Li, W. C.; Sun, Q.; Zhang, X. Q.; Lu, A. H. Dopamine as the Coating Agent and Carbon Precursor for the Fabrication of N-Doped Carbon Coated Fe<sub>3</sub>O<sub>4</sub> Composites as Superior Lithium Ion Anodes. *Nanoscale* **2013**, *5* (3), 1168–1175. <https://doi.org/10.1039/c2nr33043a>.
- (67) Pan, X.; Wang, W.; Chen, Y.; Wen, Q.; Li, X.; Lin, C.; Wang, J.; Xu, H.; Yang, L. Bio-Electrocatalyst Fe<sub>3</sub>O<sub>4</sub>/Fe@C Derived from MOF as a High-Performance Bioanode in Single-Chamber Microbial Fuel Cell. *Biochem. Eng. J.* **2022**, *187* (June), 108611. <https://doi.org/10.1016/j.bej.2022.108611>.
- (68) Zhang, C.; Liang, P.; Yang, X.; Jiang, Y.; Bian, Y.; Chen, C.; Zhang, X.; Huang, X. Binder-Free Graphene and Manganese Oxide Coated Carbon Felt Anode for High-Performance Microbial Fuel Cell. *Biosens. Bioelectron.* **2016**, *81*, 32–38. <https://doi.org/10.1016/j.bios.2016.02.051>.
- (69) Aziz, S. B.; Dannoun, E. M. A.; Murad, A. R.; Mahmoud, K. H.; Brza, M. A.; Nofal, M. M.; Elsayed, K. A.; Abdullah, S. N.; Hadi, J. M.; Kadir, M. F. Z. Influence of Scan Rate on CV Pattern: Electrical and Electrochemical Properties of Plasticized Methylcellulose: Dextran (MC:Dex) Proton Conducting Polymer Electrolytes. *Alexandria Eng. J.* **2022**, *61* (8), 5919–5937. <https://doi.org/10.1016/j.aej.2021.11.020>.
- (70) Martínez-Sánchez, B.; Cazorla-Amorós, D.; Morallón, E. Tailoring Intrinsic Properties of Polyaniline by Functionalization with Phosphonic Groups. *Polymers (Basel)*. **2020**, *12* (12), 1–18. <https://doi.org/10.3390/polym12122820>.



- (71) Du, P.; Dong, Y.; Kang, H.; Yang, X.; Wang, Q.; Niu, J.; Wang, S.; Liu, P. Graphene-Wrapped Polyaniline Nanowire Array Modified Functionalized of Carbon Cloth for High-Performance Flexible Solid-State Supercapacitor. *ACS Sustain. Chem. Eng.* **2018**, *6* (11), 14723–14733. <https://doi.org/10.1021/acssuschemeng.8b03278>.
- (72) Lu, Y.; Liu, X.; Wang, W.; Cheng, J.; Yan, H.; Tang, C.; Kim, J. K.; Luo, Y. Hierarchical, Porous CuS Microspheres Integrated with Carbon Nanotubes for High-Performance Supercapacitors. *Sci. Rep.* **2015**, *5* (July), 1–11. <https://doi.org/10.1038/srep16584>.
- (73) Sumisha, A.; Haribabu, K. Modification of Graphite Felt Using Nano Polypyrrole and Polythiophene for Microbial Fuel Cell Applications-a Comparative Study. *Int. J. Hydrogen Energy* **2018**, *43* (6), 3308–3316. <https://doi.org/10.1016/j.ijhydene.2017.12.175>.
- (74) Li, J.; Yao, C.; Song, B.; Zhang, Z.; Libonati, A. Science of the Total Environment Enrichment of Sulfur-Oxidizing Bacteria Using S-Doped NiFe<sub>2</sub>O<sub>4</sub> Nanosheets as the Anode in Microbial Fuel Cell Enhances Power Production and Sulfur Recovery. *Sci. Total Environ.* **2022**, *844* (June), 156973. <https://doi.org/10.1016/j.scitotenv.2022.156973>.
- (75) Dhillon, S. K.; Kundu, P. P. Magnesium Cobaltite Embedded in Corncob-Derived Nitrogen- Doped Carbon as a Cathode Catalyst for Power Generation in Microbial Fuel Cells. *ACS Appl. Mater. Interfaces* **2022**. <https://doi.org/10.1021/acsami.2c12279>.
- (76) Yoshii, K.; Yamaji, K.; Tsuda, T.; Matsumoto, H.; Sato, T.; Izumi, R.; Torimoto, T.; Kuwabata, S. Highly Durable Pt Nanoparticle-Supported Carbon Catalysts for the Oxygen Reduction Reaction Tailored by Using an Ionic Liquid Thin Layer. *J. Mater. Chem. A* **2016**, *4* (31), 12152–12157. <https://doi.org/10.1039/c6ta04859e>.
- (77) Tripathi, B.; Pandit, S.; Sharma, A.; Chauhan, S.; Mathuriya, A. S.; Dikshit, P. K.; Gupta, P. K.; Singh, R. C.; Sahni, M.; Pant, K.; Singh, S. Modification of Graphite Sheet Anode with Iron (II, III) Oxide-Carbon Dots for Enhancing the Performance of Microbial Fuel Cell. *Catalysts* **2022**, *12* (9). <https://doi.org/10.3390/catal12091040>.
- (78) Sun, D. Z.; Yu, Y. Y.; Xie, R. R.; Zhang, C. L.; Yang, Y.; Zhai, D. D.; Yang, G.; Liu, L.; Yong, Y. C. In-Situ Growth of Graphene/Polyaniline for Synergistic Improvement of Extracellular Electron Transfer in Bioelectrochemical Systems. *Biosens. Bioelectron.* **2017**, *87*, 195–202. <https://doi.org/10.1016/j.bios.2016.08.037>.
- (79) Champigneux, P.; Renault-Sentenac, C.; Bourrier, D.; Rossi, C.; Délia-Dupuy, M.-L.;





Bergel, A. Effect of Surface Roughness, Porosity and Roughened Micro-Pillar Structures on the Early Formation of Microbial Anodes. <https://doi.org/10.1016/j.bioelechem.2019.03.002>.

- (80) Ramasamy, R. P.; Ren, Z.; Mench, M. M.; Regan, J. M. Impact of Initial Biofilm Growth on the Anode Impedance of Microbial Fuel Cells. *Biotechnol. Bioeng.* **2008**, *101* (1), 101–108. <https://doi.org/10.1002/bit.21878>.
- (81) Khilari, S.; Pandit, S.; Varanasi, J. L.; Das, D.; Pradhan, D. Bifunctional Manganese Ferrite/Polyaniline Hybrid as Electrode Material for Enhanced Energy Recovery in Microbial Fuel Cell. *ACS Appl. Mater. Interfaces* **2015**, *7* (37), 20657–20666. <https://doi.org/10.1021/acsami.5b05273>.

